Distribution of Dark Matter in the Galaxy

A Thesis
Submitted for the Degree of
Doctor of Philosophy
in the Faculty of Science

by

Charu Ratnam

Department of Physics
Indian Institute of Science
Bangalore INDIA

Aug 1998

On the cover:

IRAS view of our Milky Way Galaxy:

This image is a composite mid and far-infrared intensity observed by the Infrared Astronomical Satellite (IRAS) in 12, 60, and 100 micron wavelength bands. The images are encoded in the blue, green, and red color ranges, respectively. Most of the emission is thermal, from interstellar dust warmed by absorbed starlight, including that in star-forming regions embedded in interstellar clouds. The image here is a mosaic of IRAS Sky Survey Atlas plates; emission from interplanetary dust in the solar system, the "zodiacal emission", was modeled and subtracted in the production of the Atlas.

Courtesy: http://www.ipac.caltech.edu

Declaration

I hereby declare that the work reported in this thesis is entirely original. It was carried out by me in the Department of Physics, Indian Institute of Science, and Indian Institute of Astrophysics, Bangalore under the supervision of Prof. R. Cowsik. I further declare that it has not formed the basis for the award of any degree, diploma, membership, associateship or similar title of any university or institution.

Prof. Ramanath Cowsik **Charu Ratnam**

Aug 1998

Dedicated
To My Parents

Acknowledgments

"No man is an Island ..."– John Donne

During the course of my Ph.D, this adage has proved to be true.

At the outset, I would like to express my sincere thanks to Prof. Cowsik for support and encouragement during the course of this thesis. I thank him for sharing some of his fun and adventures of doing science which has always been a source of delight for me. I would specially like to thank him during the writing of this thesis, for being tremendously patient and hiding signs of stress when yet another chapter arrived on his desk for comments.

I thank Pijush, who has helped me immensely with long hours of discussion and has always been patient about hearing me out.

I would like to thank Dr. S. V. Bhat and the JAP coordinators Dr. Arnab Rai Chaudhari and Dr. C. J.Jog for their support.

I take great pleasure in thanking Alex who has been a constant bundle of idiosyncrasies and cheer. I thank him for sharing some of his thoughts and for insisting on "Doing your own thing" which has proved interesting over the course of the years.

Vgopal and Rajeev for being sporting victims of my bad sense of humour and reciprocating the same. Special thanks to Kartik, Savi, Peppy and Bogart for loads of interesting food, discussions and fun.

Thanks to students of AKR's lab for having considered me part of their lab, and never denying access to their computers.

Heated arguments on a wide variety of topics with Dhruba, Alex, Santo, Kartik have been a integral part of my stay here. Special thanks to the theory group students of IISc for being helpful and fun to be with. Rajguru, Ashish and Dharam for just being good friends. I thank Mangala, Ashish and Dharam for proof-reading this thesis. K.T.Rajan, Pramila, Ramesh and Khan at the Director's office have been very helpful during the course of my stay here. I thank all the students of IIA for good cheer, during the course of my stay here.

During my stay here in IISc, I have had a lot of shop talk and help from various people including the C-Mess table, Nader, Rsidd, Amy, Kanti, Swastik, Aditi, Dandy, Debjani, Niruj and Siddharth. Gleeful thanks to Toby and Cdas for consistently loosing in Tetris games.

I take this opportunity to thank my parents for the tremendous support they have provided me and giving me the freedom to reach out to the stars.

There is a theory which states that if ever anyone discovers exactly what the Universe is for and why it is here, it will instantly disappear and be replaced by something even more bizarre and inexplicable. There is another theory which states that this has already happened.

– Douglas Adams, "The Hitchhiker's Guide to the Galaxy"

Preface

Today, there is substantial observational evidence for the presence of dark matter (DM) on all scales, and in particular the galactic scales. The rotation curves of galaxies are flat at large distances beyond the optical radii indicating the presence of large amounts of "unseen matter". While the number of galaxies with such rotation curves are large, substantiating the above conclusion, yet there has been only a limited understanding of the nature and other properties of dark matter (DM). Since DM is seen to dominate the gravitational dynamics of galactic systems understanding its properties will be a crucial input to the study of the formation of structure in the universe. The interest in the phase space structure of dark matter in general and the velocity dispersion in particular stems from the need to interpret data obtained from the laboratory experiments to detect dark matter particles. When the density distribution of all forms of matter in the Galaxy is modeled as that of an isothermal sphere the velocity dispersion is simply related to the asymptotic value of the rotational speed as $\langle v^2 \rangle^{1/2} \approx \sqrt{\frac{3}{2}} V_c(r = \infty)$. Using the value of rotational speed at the Solar neighborhood of 220 kms^{-1}yields $\langle v^2 \rangle^{1/2} \approx 270$ kms^{-1}. It should be noted that in this commonly adopted procedure, the gravitational potential of the entire Galaxy without including the individual contribution of components like the spheroid and the disc etc is described as that of a *single* component isothermal sphere. In this thesis, we would like to investigate the dynamical effect of the visible matter on the distribution of dark matter and how it affects the estimate of the velocity dispersion.

In Chapter 1 an introduction to dark matter is given with particular stress on its significance in the Galaxy. The evidence for the presence of dark matter at different length scales is reviewed. A brief overview of different candidates that stake their claim do be the particles of dark matter is also presented.

In Chapter 2 we present the self consistent model for the halo of dark matter. In order to do this we start with an assumed form for the phase-space distribution for the dark matter particles and calculate how they will be distributed when subjected to their own gravity and

that of the visible matter of the Galaxy. We have chosen two distribution functions, the Maxwellian and the King's, both consistent with stationarity to study the halo of the dark matter. The Maxwellian is essentially an isothermal distribution, with two free parameters the central density and the velocity dispersion. In the King's model the isothermal distribution is truncated at a finite value of the total energy and this translates to the so called tidal radius cut-off where the value of the density goes to zero. The emphasis of this chapter is on the fact that at small distances up to about 10 kpc the visible matter has also a very important role to play. The value of the velocity dispersion in the Solar neighborhood depends on both the visible and dark matter, and appears as one of free parameters of the problem. The value of the dark matter central density is also independently constrained by its density 0.3 GeVcm^{-3} in the local Solar neighborhood. We adopt well studied models to describe the density distribution of visible matter and proceed to solve the Poisson's equation for the dark matter, which because of the DF adopted involves both the potentials of visible matter and dark matter in a non-linear way. The self consistent dark matter potential calculated thus, yields in turn a rotation curve which is compared with the observed rotation curve of the Galaxy. The best fit between the theoretical and observed rotation curves yields a value for the velocity dispersion to be around 600 kms^{-1}which is larger than the previously obtained value of 270 kms^{-1}.

In Chapter 3 the rotation curve of the Galaxy is well measured up to a galactocentric distance of $\approx$ 8kpc with reasonable accuracy beyond which it becomes progressively uncertain and there is hardly any data beyond 20 kpc. In a recent analysis by Lynden-Bell and Lynden-Bell it was suggested that the motion of dwarf spheroidals may be used to derive the rotation curves at large distances. In this chapter we present an analysis following their suggestion. We show that the velocity distribution of dwarf spheroidals is skewed with $\langle v_t^2 \rangle = \mu \langle v_r^2 \rangle$, with μ increasing beyond the isotropic value of $\mu = 2$ to values of 5 or more because tidal disruption of dwarf spheroidals by the Galaxy has effectively removed orbits with high v_r. The data on radial velocity of the dwarf spheroidals then is used to determine the behavior of rotation curve at distances of $\approx$ 100 kpc.

In Chapter 4 we explore the consequence of the large velocity dispersion of 600 kms^{-1}derived in this thesis. The detection of any non-baryonic matter like the WIMP's involves measuring the rate of energy deposited in a laboratory detector. However to model such a rate involves specific assumptions for the number density of WIMP's, the cross-section of interaction and the velocity dispersion of the dark matter particles. In other words the rate can be written as $R = (\rho/m_{\mathrm{D}})\sigma\langle v^2 \rangle^{1/2}$, where R is the rate; ρ, the mass density, σ the cross-section of

interaction, m_D the DM mass and $\langle v^2 \rangle^{1/2}$ the velocity dispersion of the dark matter particles. The mass density around the Solar neighborhood is taken to be $0.3\,\mathrm{GeVcm}^{-3}$. Thus for any assumed mass of the WIMP particle (m_D) the bound on the cross-section is obtained by fitting the theoretical rate to the observed event rate for a given value of velocity dispersion. We obtain exclusion plots in the m_D-σ space, for the new velocity dispersion of 600 kms^{-1}. It is clear from this exercise that bounds on the scattering cross section is improved particularly for $m_D \leq 50$ GeV, because of the larger dispersion we have obtained.

In Chapter 5 we apply the model for DM-halo developed in this thesis to 12 external spiral galaxies. We choose galaxies with well studied luminosity profiles and rotation curves. Luminosity profiles are used to estimate the density distribution of the visible matter and hence the potential due to it. In terms of the model we have developed, there are two parameters defining the dark halo, that are unknown i.e ρ_{DM} and $\langle v^2 \rangle_{DM}$. The observed rotation curves of these galaxies are used to place constraints on the velocity dispersions and density of DM in these galaxies and to search for possible correlations between the visible and dark matter contents of the galaxies.

In Chapter 6 we summarize our work and discuss the results and suggest scope for further work.

Contents

1 Introduction 1

1.1 Length Scales and Dark Matter 2

1.1.1 Dark Matter in the Solar Neighborhood 2

1.1.2 Dark Matter in Galaxies 7

1.1.3 Dark Matter in Clusters of Galaxies 10

1.2 Candidates 11

1.2.1 Baryonic Dark Matter 11

1.2.2 Non-Baryonic Dark Matter 12

2 Velocity Dispersion of Galactic Dark Matter Particles 19

2.1 Theoretical Mass Models of Galaxies 20

2.2 Phase Space Distribution Functions 20

2.3 Motivation 22

2.4 Formalism 25

2.5 Models for Dark and Visible Matter 26

2.6 Numerical Procedure 29

2.7 Results 33

2.8 Discussion 36

3 Dwarf Spheroidals & Rotation Curves 42

3.1 Review of Dwarf Spheroidal Galaxies 42

3.2 Rotation Curve at Large Distances 44

3.3 Results and Discussion 46

4 Event Rates and Velocity Dispersions **54**

4.1 Detection of Dark Matter 54

4.1.1 Experiments and Detectors 56

4.2 Motivation 58

4.2.1 Theoretical Framework 59

4.3 Results and Discussion 61

5 Mass modelling and Halo Parameters of External Galaxies **68**

5.1 Observations of galaxies 68

5.1.1 Luminosity Profiles and Rotation Curves 68

5.2 Mass Modeling of the galaxies 70

5.2.1 Potentials for the Disk and Bulge 71

5.2.2 Dark Matter Potential and Trends in the Halo Parameters 74

6 Conclusions **80**

Chapter 1

Introduction

As we approach the end of the twentieth century, it has become evident that the dark matter problem is an important scientific puzzle. In the past two decades substantial observational evidence has been gathered for the presence of dark matter on various length scales. In literature pertaining to the history of dark matter it is stated that the problem often dates back to Zwicky (1933) [1] who observed the Coma cluster and based on investigations of velocity dispersions of galaxies in the cluster concluded the presence of a large amount of "missing mass". However, even before Zwicky, Kapteyn (1922) and Sir James Jean (1922) had determined the local Solar neighborhood mass density and concluded that there were 3 dark stars for every luminous star in the Galaxy. The nomenclature "dark matter" originally suggested by Kapteyn finally came to stay as did the problem of explaining the unseen mass [2]. During the same time that Zwicky made his conclusions, Oort [21] claimed that there exists substantial amount of dark matter near the Sun. After the 1930's there was a period of lull regarding this issue, which was revived by the seminal paper by Kahn and Woltjer in 1959 [4] on Local group dynamics. The key point of this paper was, the spiral galaxy, M31 which is approaching the Galaxy implied that there had to be enough mass that detached it from the Hubble flow. In 1972, Rood *et al.* [5] studied the Coma cluster and found that the cluster has a "missing mass" about a factor of seven larger than the optical mass of the galaxies in the cluster. The early HI rotation curves of spiral galaxies, which are flat at distances beyond the optical edge were obtained by Shostak & Rogstad (1973,1974) [6], Rogstad *et al.* and Seielstad & Wright (1973) [7, 8]. The observations of rotation curves of galaxies out to large radii were carried out by various people, in particular by Bosma [1], Rubin *et al.* [2, 11, 12, 13] and Faber & Gallagher (1979) [14]. A major consensus about the dynamical dominance of dark matter at galactic scale seemed to have been reached because of these two papers. In the first paper in 1974, Einasto, Kaasik and Saar [15] said, "The mass

of galactic corona exceeds the population of known stars by one order of magnitude, as do the effective dimensions" and "The mass-to-luminosity ratio rises to $f \approx 100$ for spirals to $f \approx 120$ for elliptical galaxies. With H=50 $kms^{-1}Mpc^{-1}$, this ratio is 170". Later, Ostriker, Peebles and Yahil [16] at Princeton stated, "Currently available observations strongly indicate that the mass of the spiral galaxies increases almost linearly with radius to nearly 1Mpc ... and that $f \approx 200$ M/L within the Holmberg radius".

As the presence of dark matter was gaining ground the nature of the dark matter was being speculated on. The several possible baryonic candidates included faint stars, and intergalactic gas. It soon became clear that cosmic nucleosynthesis placed strong constraints on the total amount of baryons. The baryonic mass allowed by nucleosynthesis is lower than the total dynamically estimated mass, particularly in clusters of galaxies. Thus, baryons alone will not be sufficient to close the universe; to account for an $\Omega = 1$ universe non-baryonic matter is required. The role of massive neutrinos and other weakly interacting massive particles (WIMPs) in cosmology as possible candidates for non-baryonic dark matter was first suggested as early as 1972 by Cowsik & McClelland [17, 18]. It is indeed remarkable that this has today come to stay with the recent Super-Kamiokande results confirming a lower limit for the neutrinos mass to be $\pm$ 0.07 eV.

Nothing much has really changed during the last two decades. New observations have emerged, particularly of clusters which confirm the evidence for the presence of dark matter in them. At various length scales, there exist inconsistencies between masses determined by dynamical methods and masses inferred from luminosity. These seem to threaten the various theories and existing paradigms which try to account for the observations at the smaller galactic scales and also those pertaining to cosmology in a larger context. The aim of this chapter is to emphasize the concepts, observations and ideas that concern the dark matter problem as a whole and to point out where our current understanding of this problem stands. The organization of the chapter is as follows: We begin with a review of dark matter in different scales in the Section [1.1]. We discuss the currently favoured baryonic and non baryonic candidates and the experiments to detect them in Section [1.2].

1.1 Length Scales and Dark Matter

1.1.1 Dark Matter in the Solar Neighborhood

The smallest and the nearest scale around us is the Solar Neighborhood and pioneering work to measure the total mass near the Sun was carried out by Oort [21]. The primary quantities

used to parameterize the mass in the Solar neighborhood are the Surface density (Σ) and the local density (ρ_0). Following the early analysis by Oort, Bahcall *et al.* further improved it to give the dynamical value of density $0.1 M_\odot pc^{-3}$ which implies a dark matter of $0.01 M_\odot pc^{-3}$ in the disk [19, 20, 21] of the Galaxy. Kuijken and Gilmore [22] measured a column density of 46 $M_\odot pc^{-2}$ and concluded that there was no dark matter. The local dark matter density thus remains a controversial subject today, and it is clear as we shall see further that the problem is a difficult one with possibilities for a number of systematic and statistical errors. The local halo density in units of $M_\odot pc^{-3}$ is a crucial input of the thesis at hand, hence some details here will be appropriate.

There are two approaches to the determination of the local halo density. The first approach is to make an inventory of all the objects, *i.e.*, the stars, interstellar gas and calculate the mass density due to these objects. This, by itself is quite a tedious task because of the several observational uncertainties. For example, uncertainties in detecting very low-luminosity stars even very near the Sun, uncertainties in the stellar mass-luminosity relation, uncertainties in the binary fraction of low-mass stars and uncertainties in the observed interstellar density contribute substantially to the uncertainty in the measurement of the local density. Oort compared this luminosity density with a dynamical estimate of the local density and found a discrepancy of a factor of two. In the next section we outline the method and the formalism adopted to calculate the dynamical density in the Solar neighborhood.

(i) Calculation of the local halo density

We shall now follow some of the ideas and techniques that were developed to obtain a dynamical estimate of the local density. In principle, if one just follows the dynamics of a test particle one can easily get a measure of the Galactic potential; however this an almost impossible task. The next best thing to do would be to look for a homogeneous sample of tracer stars and study their dynamics. All calculations of the mass distribution involve the collisionless Boltzmann equation (CBE), and since this is in general cumbersome one restricts oneself only to the vertical velocity moment of the CBE which is given by:

$$K_z = \frac{1}{\nu}\frac{\partial}{\partial z}(\nu\sigma_{zz}^2) + \frac{1}{R\nu}\frac{\partial}{\partial R}(R\nu\sigma_{R_*}^2) \tag{1.1}$$

where K_z is the force in the perpendicular direction, $\nu(R,z)$ is the number density of stars and σ_{zz}^2 the velocity dispersion tensor. The first term in Eq [1.1] is the dominant term of the two and therefore entails careful measurement of stellar density profiles. The σ_{zz}, to a good approximation, is described by an isothermal stellar population and taken to be independent

of height. The second term is a tricky one because it describes the tilt of the velocity ellipsoid and this term is generally ignored and this could lead to errors in the analysis of the surface density. The other crucial equation in any gravitational dynamics is Poisson's equation:

$$\nabla \cdot \vec{K} = -4\pi G\rho \tag{1.2}$$

where $\vec{K}(R,z)$ is the gravitational force in an axisymmetric Galaxy , and ρ is the density of gravitating matter. Writing Eq [1.2] explicitly and replacing the R-gradient $\nabla \cdot \vec{K}$ in terms of V_c, the rotational velocity of the Galaxy we obtain:

$$\rho = -\frac{1}{4\pi G}\left[\frac{\partial K_z}{\partial z} + \frac{1}{R}\frac{\partial (V_c^2)}{\partial R}\right] \tag{1.3}$$

Further, the surface density can be written as:

$$\Sigma(z) = \int_{-|z|}^{|z|} \rho(z)dz \approx \frac{|K_z|}{2\pi G} \tag{1.4}$$

It is clear from Eqs [1.1-1.3] that a direct estimate for the density ρ_0 depends on the square of distance-scale errors since it is derived from the second derivative of the stellar space distribution. From Eq [1.4], we see that the surface density is only linearly dependent on the stellar distribution. Plugging in direct observables will lead to erratic and incorrect answers, consequently special methods of analysis are needed.

Oort combined Eq [1.1] (neglecting the second term) and Eq [1.2] to obtain:

$$\frac{\partial}{\partial z}\left[\frac{1}{\nu}\frac{\partial (\nu\sigma_{zz}^2)}{\partial z}\right] = -4\pi G\rho \tag{1.5}$$

If the number density $\nu(R,z)$ and the mean square vertical velocity σ_{zz}^2 of any population of stars is known then Eq [1.5] can be used to calculate the local mass density ρ. Oort used this equation for different sets of stellar populations and obtained an average value of $\rho_0 = 0.15 M_\odot pc^{-3}$ for density in the Solar neighborhood and this is called the Oort limit in his honour. This analysis involves triple differentiation; the first to obtain the star counts $\nu(z)$ and the next two to satisfy the Eq [1.5].

Bahcall tried to reduce this uncertainty of triple differentiation by assuming an isothermal decomposition of all the known contributors to mass and therefore σ_{zz}^2 to be independent of z. Neglecting the second term in Eq [1.1], the density of the i^{th} isothermal component satisfies:

$$\rho(z_i) = \sum_{i=1}^{N_{iso}} \rho_i e^{-\Phi(z_i)/\sigma_{zz,i}^2} \tag{1.6}$$

The Poisson Eq [1.2] can be written as

$$\frac{d^2\Phi}{dz^2} = 4\pi G(\rho_{\rm disk} + \rho_{\rm halo}) \tag{1.7}$$

Bahcall solved this equation by further assuming that the velocity dispersion for the observed and unobserved components are the same and subsequently the equation can be written as:

$$\frac{d^2\Phi}{dz^2} = 4\pi G\rho_{\rm obs}(0)\left(\sum_{i=1}^{N_{obs}} A_i e^{-\Phi/\sigma_{zz}^2} + \sum_{j=1}^{N_{unobs}} B_j e^{-\Phi/\sigma_{zz}^2} + \epsilon\right) \tag{1.8}$$

The quantities on the right hand side of the equation are made dimensionless and normalised with respect to $\rho_{obs}(0)$. From Eq [1.8] we see that the density is decomposed to N observable and unobservable components with $A_i = \rho_i(0)/\rho_{\rm obs}(0)$, with B_j, the unobserved mass fraction also defined similarly as the ratio of the mass density in the component j to the total observed mass density. ϵ is defined as the ratio of the effective halo mass density to the total observed mass density. Thus $\epsilon = \rho_{\rm halo}^{eff}/\rho_0^{\rm obs}$ where:

$$\rho_{\rm halo}^{eff} = \rho_{\rm halo}(R) - \frac{\partial}{\partial R}V_c^2(R) \tag{1.9}$$

On specifying a set of observable mass components with their velocity dispersions ($\sigma_{zz,i}$), and their relative densities (ρ_i), and using the appropriate boundary conditions, Φ is determined. Further assumptions regarding the unobserved matter are made. The models are such that it is assumed that the unobserved matter is distributed in proportion to the stars or the ISM (InterStellar Medium), *i.e.*, $B_j = PA_i$ where P could be P_{ISM} or P_{stars}. Various input values of P and ϵ and σ_{zz} were chosen and corresponding models were obtained. Bahcall then fit the distribution of F-stars and K-stars [21] reported by Hill, Hilditch and Barnes [23] to infer a total mass density of $0.1 M_\odot pc^{-3}$ and column density of 30 $M_\odot pc^{-2}$. He also reanalyzed the available F-dwarf and K-giant high galactic latitude data in these models which are self-consistent, in the sense that the matter which generates the gravitational field itself responds to it through the CBE. The conclusions he reached were,"the amount of *unobserved* material is the disk is at least as large as 50% of the observed material for all the models that are discussed". Bahcall's analysis is a more robust measure for density than the surface density, because as mentioned earlier the former involves the second derivative of the observed star count data. Thus the available values for the mass density near the Sun remain limited by the systematic and random difficulties with the available data.

(ii) Calculation of the local surface density

Kuijken and Gilmore used an entirely different approach in estimating the surface density of mass near the Sun. Their approach involves a maximum likelihood comparison of the observed and predicted distribution function ($f(z, v_z)$). The density gradient is a well measured quantity and this information is used to derive the velocity distribution in the various model potentials. The density can be written as

$$\rho(z) = \int_{-\infty}^{\infty} f_z(z, v_z) dv_z \tag{1.10}$$

$$= 2\int_{\Phi}^{\infty} \frac{f_z(E_z)}{\sqrt{2(E_z - \Phi)}} dE_z \tag{1.11}$$

and using the Abel transformation we can write

$$f_z(E_z) = \frac{1}{\pi}\int_{E_z}^{\infty} \frac{-d\rho/d\Phi}{\sqrt{2(\Phi - E_z)}} d\Phi \tag{1.12}$$

so, there is a unique relation between $\rho(\Phi)$ and $f_z(E_z)$. As seen from the above equations, $f_z(E_z)$ depends on the density only at points where the potential exceeds E_z, *i.e.*, beyond the point $z = \Phi(E_z)^{-1}$. This is crucial since the potential at large distances from the plane of the galaxy can be derived from the high z-data alone. It is this property which constrains K_z, the force in the perpendicular direction to the Galactic plane Eq [1.2], quite well at large z despite poorly known mass distribution at low z. While Bahcall's analysis involved making an isothermal assumption for the tracer sample of stars, Kuijken and Gilmore instead choose different model potentials to derive $f_z(v_z, z)$, given the density distribution $\rho(z)$ which is a well observed quantity. This derived distribution function is directly compared to the observed distribution function in the (z, v_z) plane.

The force K_z is directly related to the surface density. The essential features of the K_z are quantified as

$$-K_z = 2\pi GK\frac{z}{\sqrt{z^2 + D^2}} + 4\pi GFz \tag{1.13}$$

and the corresponding potential is given by

$$\Phi(z) = 2\pi GK\sqrt{(z^2 + D^2)} - D + 2\pi GFz^2 \tag{1.14}$$

In Eq [1.14], the first term corresponds to a disk and K corresponds to the disk density and D the scale height. F measures the large z quadratic term in the potential, which is predominantly caused by the halo density. Therefore F behaves like a constant halo density term. Using the model potential (Eq [1.14]) and the $\rho(z)$ data with rotation curve constraints

yields predicted values for the $f(z, v_z)$. A maximum likelihood analysis was carried out with the predicted and observed distribution of velocities which in turn was used to obtain the values for the parameters of the potential. This analysis leads to a value for K_z which corresponds to $46 \pm 9 M_{\odot} pc^{-2}$ (using Eq [1.4]) for the surface density. The same authors integrated the local "observed" density to obtain a surface mass density of $48 \pm 8 M_{\odot} pc^{-2}$. Comparing these two values led them to conclude that there is no disk dark matter. In their reanalysis in a later paper Kuijken and Gilmore [24] reported the above value for the surface density plus an additional $25 M_{\odot} pc^{-2}$ in a dark halo below $z < 1.1$ kpc.

There are several others who have been working on the dynamical determination of the local halo density. Bienaymé, Robin, & Creze [25] inferred a local halo density of $64 \pm 12 M_{\odot} pc^{-2}$. They regarded this is as consistent with no dark matter, but if dark matter were allowed the best fit would be of the order if the scale height is $h \approx 600$pc. Bahcall, Flynn and Gould [26] analyzed a cone of K giants and found $\Sigma_0 = 85 \pm 25 M_{\odot} pc^{-2}$. These discrepancies perhaps indicate the systematic uncertainties in the different analysis procedure. The analysis due to Bahcall assumes that the $\rho_{\rm DM} \propto \rho_{\rm stellar}$ and this is of special relevance, perhaps to baryonic dark matter (DM) in the form of low mass stars like brown dwarfs, which may have the same σ_{zz} as the other stars, and hence expected to have similar z-distribution.

1.1.2 Dark Matter in Galaxies

(i) Rotation curves: kinematics and observation

The rotation curve is a good tracer of the mass distribution of spiral galaxies [27]. In most galaxies light falls of exponentially; assuming mass traces light, one would expect that the rotation curve for most galaxies should fall have a Keplerian fall off at the optical edge of the galaxy. However, observational evidence indicates that the rotation curve for spiral galaxies is flat or gently rising beyond the optical edge [1, 2, 9, 28]. In this section we shall review some of the literature on the rotation curve of our Galaxy.

The rotational velocity, of any test object assumed to be in circular orbit around the Galaxy is usually measured as a function of the distance from the center. Any object in the Galaxy as seen from the barycenter of the Solar system, will have both radial and transverse components of motion v_t and $v_{\rm R}$ because of the differential rotation of the Galaxy . The Fig [1.1] indicates the various distances and angles that are used to derive the basic expression for the radial and transverse velocity, where

Figure 1.1: Galactic rotation velocities and their projections along the line of sight. S=Sun, C=Galactic Center, V_0= Sun's velocity, V = Velocity of the star/test object. R_0=distance between Sun and Galactic Center, l= galactic longitude. PT= $R\sin\alpha$; ST=$R_0\cos\alpha$

The equations for v_R and v_t can be derived with the help of the Fig [1.1]. The subscript zero refers to the solar neighborhood. The Fig [1.1] shows an object at P, a distance r from the Sun and at a longitude l. Then

$$v_R = V\sin\alpha - V_0\cos l \tag{1.15}$$

$$v_t = \frac{V}{R}(R_0\cos l - r) - V_0\cos l \tag{1.16}$$

$V(R)$ is the rotational velocity of the object in a circular orbit. The above equation can also be rewritten in terms of the angular velocities $w = V/R$. The equation for the radial velocity is the most crucial as the observations yield radial velocity measurements which are used for deriving the rotation curve. For the near neighborhood of the Sun these two equations can be approximated so that they depend only on the local characteristics of Galactic rotation. The star is in the local solar neighborhood, therefore the approximation $|R - R_0| \ll R_0$ is valid. Substituting in the earlier equation we obtain,

$$v_R = \left[\frac{V_0}{R_0} - \left(\frac{dV}{dR}\right)_0\right] r\sin l\cos l \tag{1.17}$$

$$= Ar\sin 2l \tag{1.18}$$

where

$$A = \left(\frac{1}{2}\right)\left(\frac{V}{R} - \frac{dV}{dR}\right)_0$$

$$v_t = \left[\frac{V_0}{R_0} - \left(\frac{dV}{dR}\right)_0\right] r\cos^2 l - \frac{V_0}{R_0} \tag{1.19}$$

$$= r(A\cos 2l + B) \tag{1.20}$$

where

$$B = -\frac{1}{2}\left(\frac{V}{R} + \frac{dV}{dR}\right)_0$$

A and B are the well known Oort's Constants. Together, they determine the local angular velocity and the local slope of the rotation curve. In terms of the angular velocities, Eq [1.19] can be rewritten as

$$v_R = R_0(w - w_0)\sin l \tag{1.21}$$

According to this equation the observed radial velocity must be greatest at the point where w differs most from w_0. For any well behaved density distribution w must fall off monotonically with increasing R; hence the velocity extremum will correspond to the value of w where the line of sight comes closest to the Galactic center. From Fig [1.1], it is clear that at this point $R = R_0 \sin l$. w is obtained by substituting this maximum velocity in Eq [1.19]. This method is often referred to as the tangent point method, because at the point of extremum velocity the line of sight is tangent to a circle with $R = constant$.

Measurement of the Galactic rotation curve in the outer parts of the Galaxy generally requires the determination of independent distances and velocities to a set of objects or clouds of gas. The luminous main sequence stars and HI profiles are frequently used for this purpose. For luminous main sequence stars the exciting stars of either the HII regions or reflection nebulae are identified and their distances are determined from spectroscopic parallaxes [3, 4, 32, 33]. Velocities are determined accurately from associated CO clouds. Planetary nebulae, carbon stars and Cepheid variables are standard candles which are used to obtain rotation curves [34, 35, 36, 37, 38]. In determination of rotation curves from HI lines the velocity is observed directly from the Doppler shift and has a small uncertainty. In such observations it is necessary that the parcels of gas are coherent and share similar distances from the center. Merrifield [39] successfully accomplished this by assuming that the Galaxy is asymmetric; he used the radial velocity of the HI to find the gas in a ring of constant Galactic radius. The angular scale height of the gas is determined at different longitudes and distance to the

HI ring was found by the variation of its angular height across the sky. Since the HI layer extends beyond the optical disk, the rotation curve can be determined beyond the optical edge. All these measurements indicate that the rotation curve is flat, and not declining as one would expect if all the mass contribution came only from the stars.

(ii) Dark Matter in external galaxies

The main efforts are to quantify the the amount of dark matter and its distribution in the external galaxies. HI observations provide the evidence for dark matter in external galaxies. The need for dark matter stems for two reasons: i) there is a mismatch between the observed rotation curve and one calculated from the "visible" matter alone, assuming constant mass-to-light ratio, and ii) the mismatch is larger when the rotation curve extends to larger distances. The most debatable step in this analysis is the relative contribution of the disk and the halo to the rotation curve, or the mass-to-light ratio. Work has been proceeding rapidly since the rotation curves of 967 spiral galaxies were presented by Persic and Salucci [40].

Recently there have been couple of approaches to study the problem in elliptical galaxies. The first approach uses stellar kinematics to trace the potential. The second method is to use the HI component and ionized component of the disks as a tracer of the potential [41, 42]. Comparison of M/L for the spirals and ellipticals seem to show the same trend when the radial distance is normalized [43].

1.1.3 Dark Matter in Clusters of Galaxies

Rich clusters of galaxies containing large amount of hot gas can be used as powerful tools to constrain the nature and amount of dark matter. Traditionally, the velocity dispersion of galaxies is used to calculate the binding potential of the clusters using the virial theorem [1]. After Zwicky's seminal paper, Rood *et al.* measured the radial velocities for 40 galaxies in the Coma cluster and concluded that the cluster M/L ratio was of the order of 250. Multiwavelength studies have been carried out to measure the mass distribution in the clusters: The optical data gives a measure of the galaxy velocity dispersion (σ) and the X-ray data provides an estimate of the intracluster gas temperature (T). On assuming that the gas and galaxies are in hydrostatic and isothermal equilibrium, one obtains a relation between the σ (velocity dispersion) and T(Temperature) to be $\sigma \propto T^{0.5}$. A strong correlation between σ and T was observed, *i.e.*, $\sigma = 332 \pm 52\ (kT/\mu m_p)^{0.6\pm0.1}\mathrm{kms}^{-1}$ [44], where μm_p is the molecular weight of the gas. This implies that the gas and galaxies in the cluster trace the same potential

and also justifies the assumptions of isothermal and hydrostatic equilibrium. Distortion of background galaxies due to lensing by the intervening cluster, can also give a measure of the mass of the cluster. These two independent ways of mass determination are found to be consistent with each other.

The cluster mass calculated is of the order of $10^{14} - 10^{15} h^{-1} M_{\odot}$ [45]. The mass-to-light ratio of 300 for a large number of rich clusters, implies a dynamical value of $\Omega = 0.2$, within a cluster radius of 1Mpc. The X-ray emitting gas contributes 30% of the cluster mass within $1.5h^{-1}$ Mpc of a rich cluster [46]. Standard nucleosynthesis limits $\Omega_b \leq 0.06$ which means that the baryon fraction in clusters is larger than that predicted by nucleosynthesis. These results have been interpreted to mean that either Ω is less than the critical value or that baryon fraction is larger than that predicted by standard model nucleosynthesis [47].

1.2 Candidates

It is clear from the earlier section that there is very strong evidence for the presence of dark matter on various scales. The most secure evidence for dark matter, which is in the halos of spiral galaxies contributes to Ω roughly between 0.03 and 0.1 [1, 2]. On larger scales like clusters the contribution to Ω is probably between 0.03 and 0.2 [45]. All detection experiments are geared towards detecting Galactic DM (dark matter). The obvious question to address now is the nature of dark matter.

The candidates for dark matter are faint stars, interstellar gas in the baryonic DM and WIMPs, axions and neutrinos which fall into the non-baryonic category. We shall discuss each of these candidates and outline some of the on-going experiments that are being done to detect them.

1.2.1 Baryonic Dark Matter

It is clear, that while there are baryons that are luminous there is also a possibility that a substantial number of them are "dark". Dark baryons are generally thought to be in the form of low mass stars called MACHOS (MAssive Compact Halo ObjectS) like brown dwarfs or Jupiter like planets, Recently, Pfenninger and Combes suggested the cold molecular clouds could be plausible dark matter candidates. Low luminosity stars as possible candidates for dark matter have been ruled out by a recent HST observation by Bahcall *et al.* [48]. They concluded that these stars contribute less that 6% of unseen matter.

Paczyński [49] proposed the idea of using gravitational micro-lensing to detect massive dark

objects in our galaxy by monitoring the brightness of stars in the Magellanic clouds. The basic physics of microlensing is quite simple. If light passes very close to the line of sight to a foreground star, the light will be deflected to produce two images of the background star. In the case of perfect alignment the star will appear as an "Einstein ring" with a radius of

$$r_E = \sqrt{\frac{4GMLx(1-x)}{c^2}} \tag{1.22}$$

where M is the lens mass, L is the observer-source distance and x is the ratio of the observer lens and observer source distances. For a source distance of 50 kpc and a lens distance of 10 kpc, it yields a resolution of ≈ 0.001 arcsecond which is superior to the Space Telescope resolution and hence the term "microlensing". However, in the point source approximation, the lensing produces a net amplification of the luminosity, which can be quite large. Since objects in the Galaxy are in relative motion, this amplification will be time dependent; for a typical lens with a typical transverse velocity of 200 kms^{-1}, the duration is of the order of days. The number of stars that will be lensed is only one in two million per day and hence this method requires careful monitoring of stars.

Microlensing searches can give definitive results on dark matter objects in the mass range of 10^{-9} to $10^4 M_\odot$. There are various experiments involved in determining the MACHO fraction in the Galaxy and their corresponding mass. The MACHO [50] collaboration has the exclusive use of a 1.3 m telescope at Mt. Stromlo for 4 years. Using a dichroic filter they take exposures in the red and blue with a field of view of about 0.5 deg^2. They target both the LMC and the Galactic bulge. The French collaboration EROS [51, 52] uses a 0.4 meter telescope with a field of view is also 0.5 deg^2. The OGLE [53] group does not have a telescope of its own, instead it uses the 1 meter telescope at Las Campanas with a field of view of 0.06 deg^2. Under assumptions of a spherical halo, it has been found that the eight microlensing events found so far imply a halo MACHO fraction as high as 50% and an average mass of $0.27 M_\odot$. However this conclusion should be taken with some caution because the statistics of these events are low and also the mass depends very strongly on the "standard model" for the halo.

1.2.2 Non-Baryonic Dark Matter

At the time of writing the thesis, the Super-Kamiokande has confirmed the existence of neutrinos with non-zero mass. As mentioned earlier WIMPs (Weakly Interacting Massive Particles) and axion can be considered as non-baryonic dark matter, alongside the neutrinos. We shall discuss each of these candidates briefly here.

(i) Neutrinos

In the standard Big Bang model copious amount of neutrinos are produced and the universe today is filled with thermal neutrinos at 1.7K. If neutrinos have a non-zero mass then they will contribute substantially as dark matter particles, to the mass density of the universe. The first suggestion of neutrinos, and indeed any nonbaryonic candidate contributing to the Ω came from Cowsik & McClelland [17]. There are experiments which put an upper limit on the neutrino mass as [54]:

$$\begin{aligned} m_{\nu_e} &< 15\text{eV} \\ m_{\nu_\mu} &< 0.17\text{MeV} \\ m_{\nu_\tau} &< 24\text{MeV} \end{aligned}$$

The Super-kamiokande experiment has recently announced that the mass deficit of the neutrinos is ± 0.07 eV, confirming the fact that neutrinos have mass. This result is exciting since it offers for the first time one of the most concrete candidate for the dark matter problem. The Super-kamioka detector consists of a huge 50,000 ton double layered tank containing ultra pure water, monitored by thousands of photo multipliers. Located in a mine beneath the Japanese 'Alps', near the town of Kamioka, the project has been collecting data for the past two years. Charged particles traveling at speed large than that of light in water emit Cerenkov light which is collected by the photo multipliers. The pattern, timing and intensity of these light pulses allows one to determine the particle's direction, energy and identity. Super-Kamioka has observed is the muon neutrino oscillating though it has not yet determined the to which state it oscillates.

(ii) WIMPs

Among the candidates for the dark matter particles are the WIMPs whose energies range from a few GeV to TeV. They are a generic class of particles predicted from various supersymmetric models are the cold dark matter particles [2]. They are so called, because they were non-relativistic at the time of decoupling in the early phases of the universe. The interaction cross-section (σ) of these particles is not known, however an order of magnitude estimate can be made.

This information on σ is crucial to the plan and design of experiments searching for these particles. The argument due to Lee and Weinberg is as follows [56]: In the early universe the

temperatures are large and there is thermal equilibrium ($m_{WIMP} \gg kT$) maintained between the WIMPs and other particles like the leptons. However when the universe expands and temperature falls below $m_{WIMP}/20$; the particles are no longer in equilibrium. Two things can then happen: if the annihilation rate is much faster than the expansion of the universe, the WIMPs will disappear. However if the annihilation rate is smaller than the expansion rate then there will be an abundance of the WIMPs that will remain. For a typical WIMP mass in the GeV region the annihilation cross section is given by

$$\sigma v = \frac{10^{-26}\text{cm s}^{-1}}{\Omega_{WIMP}h^2}$$

where h is the the Hubble's constant normalised to lie between 1/2 and 1. It is interesting to note, that for $\Omega = 1$ the interaction cross section is roughly of the weak interaction scale.

There are basically two methods for detecting WIMPs: direct detection which is due to elastic scattering of the WIMP on the detector [5], and indirect detection which involves further annihilation of the WIMPs within the sun or earth which may be detectable as a high neutrino flux. There are various problems in direct detection, mainly because of the low signal and high background noise. The energy deposited is small for the mass range of the WIMP involved. The expected event rate is small because of the small cross section of interaction. The best confirmation for a WIMP would come from the annual and diurnal motion of the earth with respect to the sun which results in a change in the recoil energy spectrum. We shall discuss some of the experiments n a later Chapter.

(iii) Axions

Axions are alternatives to the WIMPs as candidates for dark matter. They are much lighter than the SUSY (SuperSymmetric) relics, and are produced by a different mechanism. They were first proposed to explain the lack of CP violation in strong interactions. Although the interactions of axions with ordinary matter is very weak, Sikvie [58] proposed a method of detection of Galactic axions. The axion has a weak coupling to the photons. Therefore if one immerses a resonant cavity in a strong magnetic field, Galactic axions, which pass through the cavity, may be converted to fundamental excitations of the cavity and may therefore become observable. The typical allowed window range for the axions is $10^{-2} - 10^{-4}$ eV and it should be kept in mind that there are no accelerator tests for axion in this mass range.

There has been no shortage of proposed candidates since the advent of the dark matter problem nearly seventy years ago. The neutrinos, WIMPs and the axion are the only ones

that have survived theoretical scrutiny so far. However it is important to bear in mind that although very attractive, the ideas regarding the WIMPs and axions are still speculative. It is a tough experimental challenge, and the discovery of particle dark matter will revolutionize both particle physics and cosmology.

While the nature of dark matter is not definitely known the idea is to put dynamical constraints on the dark matter properties by observations of visible matter. On galactic scales the rotation curve constrains the density distribution of dark matter at large distances. On smaller scales the visible and the dark matter together conspire to produce a rotation curve. The work presented in this thesis relies on the observational data in the form of rotation curve and imposes constraints on the velocity dispersion of these particles. We also discuss the effect of this dispersion on the detection of DM.

Bibliography

[1] Zwicky, F., 1933, Helvetica Physics Acta, 6, 110

[2] Trimble, V., 1994 in *AIP Conference Proceedings, 336 on Dark Matter*, eds. Stephen S. Holt, & Charles L. Bennett, 57

[3] Oort, J.H., 1932, BAN, 6, 249

[4] Kahn, F.D., & Woltjer, L., 1959, ApJ, 130, 705

[5] Rood, H.J., Page, T.L., & Kintner, E.C., 1972, ApJ, 175, 627

[6] Shostak, G.S., & Rogstad, D.H., 1973, A&A, 24, 411

[7] Seielstad, G.A., & Wright, M.C.H., 1973, ApJ, 184, 343

[8] Rogstad, D.H., Shostak, G.S., & Rots, A.H., 1973, A&A, 22, 111

[9] Bosma A., 1978, Ph.D. Thesis, University Of Groningen

[10] Rubin, V.C., Ford, K., & Thonnard, N., 1978, ApJL, 225, L107

[11] Rubin, V.C., Ford, K., & Thonnard, N., 1980, ApJ, 238, 471

[12] Rubin, V.C., Ford, K., Thonnard, N. & Burstein, D., 1982, ApJ, 261, 439

[13] Rubin, V.C., Ford, K., & Thonnard, N., 1985, ApJ, 289, 81

[14] Faber, S.M., & Gallagher, J.S., 1979, ARA&A, 17, 135

[15] Einasto, J., Kaasik, A., & Saar, E., 1974, Nature, 250,309

[16] Ostriker, J.P., Peebles, P.J.E., & Yahil, A., 1974, ApJL, 193, L1

[17] Cowsik, R., & McClelland, J., 1972, Phys.Rev.Lett., 29, 669

[18] Cowsik, R., & McClelland, J., 1973, ApJ, 180, 7

[19] Bahcall, J.N., 1984a, ApJ, 276, 156

[20] Bahcall, J.N., 1984a, ApJ, 276, 169

[21] Bahcall, J.N., 1984a, ApJ, 287, 926

[22] Kuijken, K., & Gilmore, G., 1989a, MNRAS, 239, 571

[23] Hill, G., Hilditch, R.W., & Barnes, J.V., 1979, MNRAS, 186, 813

[24] Kuijken, K., & Gilmore, G., 1991, ApJL, 367, L9

[25] Bienaymé, O., Robin, A., & Crézé. M., 1987, A&A 180, 94

[26] Bahcall, J.N., Flynn, C., & Gould, A., 1992, ApJ, 389, 234

[27] King, I.R., 1989, in 19^{th} SAAS-FEE course on *The Milky Way as a Galaxy*, eds., Gilmore, G., King. I.R., & Van Der Kruit, P.103

[28] Begeman, K.G., 1987, Ph.D. thesis, University of Groningen

[29] Kent, S., 1986, AJ, 91, 1301

[30] Blitz, L., 1979, ApJL, 231, L115

[31] Fich, M., Blitz, L., & Stark A. A., 1989, ApJ, 342, 272

[32] Jackson, P.D., Fitzgerald, M.P., & Moffat, A.F.J., 1979, in *The Large-Scale Characteristics of the Galaxy*, eds., Burton, W.B., Reidel: Dordrecht, 221

[33] Brand, J., & Blitz, L., 1993, A&A, 275, 67

[34] Schneider, S.E., & Terzian, Y.,1983, ApJL, 274, L61

[35] Schechter, P., Aaranson, M., Cook, K.H., & Blanco, V., 1988, in *The Outer Galaxy*, eds., Blitz & Lockman, Springer: New York, 31

[36] Aaranson, M., Blanco, V., Cook, K.H., & Schechter, P.L., 1989, ApJS, 70, 637

[37] Caldwell, J.A.R., and Coulson, I.M., 1987, AJ, 93, 1090

[38] Welch, D., 1988, in *The Mass of the Galaxy*, eds., Fich, M., CITA: Toronto, 68

[39] Merrifield, M.R., 1992, AJ, 103, 1552

[40] Persic, M., & Salucci, P., 1995, ApJS, 99, 501

[41] Bertin, G., Saglia, R.P., & Stiavelli, M., 1992, ApJ, 384, 423

[42] Dejonghe, H., 1989, ApJ, 343, 617

[43] Van der Marel, R.P., 1991, MNRAS, 253, 710

[44] Lubin, L.M., & Bahcall, N.A., 1993, ApJL, 415, L17

[45] Bahcall, N.A., & Lubin, L.M., 1994, ApJ, 426, 513

[46] Briel, U.G., Henry, J.P., & Bohringer, H., 1992, A&A, 259, L31

[47] Bahcall, N. A. 1994, *AIP conference proceedings on Dark Matter*, eds., Stephen S. Holt and Charles L. Bennett, 201

[48] Bahcall, J.N., Flynn, C., & Gould, A., 1994, ApJL, 435, L51

[49] Paczyński, B., 1986, ApJ, 304, 1

[50] Alcock, C., Akerlof, C.W., Allsman, R.A., Axelrod, T.S., Bennett, D.P., Chan, S., Freeman, K.C., Griest, K., Marshall, S.L., Park, H.S., Perlmutter, S., Peterson, B.A., Pratt, M.R., Quinn, P.J., Rodgers, A.W., Stubbs, C.W., & Sutherland, W., 1993, Nature, 365, 621

[51] Renault, C. *et al.* , astro-ph/9612102

[52] Aubourg, E. *et al.* , 1993, Nature, 365, 623

[53] Udalski, A., *et al.* , 1993, Acta Astronomica, 43, 289

[54] Particle Data Group, Barnett, R.M., *et al.* , 1996, Phys.Rev.D., 54, 1

[55] Jungman, G., Kamiokowski, M., & Griest, K., 1996, Phys. Rep., 267

[56] Lee, B.W.,& Weinberg, S., 1977, Phys.Rev.Lett., 39, 165

[57] Beck, M. *et al.* , 1994, Phys. Lett. B., 336, 141; Caldwell, D.O. *et al.* ., 1988, Phys. Rev. Lett., 61, 510

[58] Sikivie, P., 1983, Phys. Rev. Lett., 51, 1415

Chapter 2

Velocity Dispersion of Galactic Dark Matter Particles

In the earlier chapter we concluded that there is definite evidence for the presence of dark matter on various scales. As yet, the distribution and nature of dark matter remain inconclusive. The problem at hand is a serious one and a maiden attempt to approach the problem at the galactic scale [1], more so in the Milky way has already been made. The observations of the rotation curve [2, 3, 4] in the Milky way provide ample evidence for the presence of dark matter.

Most of the theoretical attempts so far in describing the dark matter in galaxies have been on obtaining "mass models" for the dark matter component of the Galaxy and fitting it to the rotation curve [5]. The customary approach to obtain the overall potential field has been, to assume that the Galaxy is comprised of several components and the density distribution of each is adjusted to get the best fit to the rotation curve. Our approach has been to start from an assumed form for the phase space distribution for the dark matter component of the Galaxy and obtain a theoretical rotation curve. Comparison of the theoretical rotation curve with the observed one yields the halo parameters as best-fit values. This approach is interesting in that it addresses the for the first time the determination of the velocity dispersion as a problem and also succeeds in laying down a formalism for determining this value.

We discuss the customary approach of modelling the mass distribution in Section [2.1]. We introduce the current theoretical work, reviewing some properties of phase space distribution functions in the Section [2.2]. We describe the main work of the thesis, the new results that emerge from our study and their implications in Sections [2.3-2.8]

2.1 Theoretical Mass Models of Galaxies

The general approach to modelling the mass of spiral galaxies, has been to assume various components in the galaxy and manipulate the density distribution such that the potential field induced by them, fits the observed rotation curve. At small distances, the rotation curve is modelled by the visible matter distribution which consists of the bulge and disk. If these were the only two components comprising the galaxy, then the rotation curve at large distances would fall off as function of the galactocentric radius. Observations of galaxies, however, show a gently rising or flat rotation curve at distances beyond the visible edge of the galaxy. To account for the flat rotation curve, another massive component, a halo with an isothermal density distribution is added.

The earliest mass models was given by Schmidt (1956) and since then there have been various models for the Galaxy [5, 6, 7]. Bahcall *et al.* [6] use a spherical mass distribution for the bulge, an exponential disk and a spherical distribution for the halo.

While, in general, three components are required to explain the observed rotation curve, the relative contribution of each of these components to the rotation curve is unknown. There have been efforts to point out that probably a "maximum disk" model is at work which does not require a dark halo to fit the rotation curve, for may be a few of the galaxies [8]. According to this model the disk is assumed to contribute dominantly to the inner part of the galaxy rotation curve. The fitting procedure is as follows: the circular velocity due to the disk and bulge can be obtained from the observed luminosity profile. making assumptions about the value of $(M/L)_{\text{disk}}$. The largest possible value, which is consistent with the rotation curve is assumed. Then the halo with an appropriate density distribution is added. The value of $(M/L)_{\text{disk}}$ is changed until the final best fit to the rotation curve is obtained. The process starts with the largest possible value for $(M/L)_{\text{disk}}$, which is then decreased to accommodate the halo. The final solution, therefore, still has the largest possible $(M/L)_{\text{disk}}$ value which is the maximum disk fit [9].

2.2 Phase Space Distribution Functions

The advantages of using the phase space distribution function (DF) formalism to the study the Galaxy is two-fold. The idea is to study the motion of the stars comprising the Galaxy and use the fact that every star that travels through the phase space has some information of the place it visited. It is then possible to get information about far off places in the Galaxy

from a local analysis of variables like density or velocity dispersion. The other advantage from the point of view of this thesis is that the velocity dispersion appears as a free parameter in the phase space distributions we have chosen to study.

The equation governing the phase space DF f goes by the name "Collisionless Boltzmann Equation" (CBE) or the "Liouville equation". This equation is often referred to as the continuity equation followed by the stars. In Cartesian coordinates this can be written as

$$\frac{df}{dt} = \frac{\partial f}{\partial t} + u\frac{\partial f}{\partial x} + v\frac{\partial f}{\partial y} + w\frac{\partial f}{\partial z} - \frac{\partial \Phi}{\partial x}\frac{\partial f}{\partial u} - \frac{\partial \Phi}{\partial y}\frac{\partial f}{\partial v} - \frac{\partial \Phi}{\partial z}\frac{\partial f}{\partial w} = 0 \tag{2.1}$$

where (x,y,z) are the position and (u,v,w) the velocities of the star and Φ represents a smooth potential for the Galaxy. This equation states that along the path of any star in phase space the total derivative of f is zero. In other words as the point representing the star moves along the phase space, the density around it remains a constant.

Since Eq [2.1] is a first order linear partial differential equation in n-variables and the general solution is not known. The equation can be reduced to $n-1$ ordinary differential equations. The solution is to find the $n-1$ integrals of these ordinary differential equations. Let the integrals I, be expressed in the form:

$$I_i(x_1, x_2, ...x_n) = const., \qquad i = 1, 2, ..n-1 \tag{2.2}$$

The general solution to the CBE is then given as:

$$f(x_1, x_2 ... x_n) = G(I_1, I_2, I_3 ... I_{n-1}) \tag{2.3}$$

Thus the general solution of the CBE requires that f, the distribution function be expressed as a function of G of the integrals of motion of the star. In the time independent situation these equations can be reduced to what are known as "subsidiary equations":

$$\frac{dx}{u} = \frac{dy}{v} = \frac{dz}{w} = \frac{du}{-\partial\Phi/\partial x} = \frac{dv}{-\partial\Phi/\partial v} = \frac{dw}{-\partial\Phi/\partial z} \tag{2.4}$$

These equations are the equations of motion of a star and it is clear from these equations that one integral of motion is the energy integral given by

$$I_1 = E = \frac{1}{2}(u^2 + v^2 + w^2) + \Phi(x, y, z) = const \tag{2.5}$$

If the potential is independent of time, this integral always exists. Thus,

$$f(x, y, z, u, v, w) = F(I_1) \tag{2.6}$$

Another example of isolating integral is when the potential is axisymmetric then one of the integrals of motion is the angular momentum. Suppose we consider this as the other integral I_2 then this motion is also confined to a particular I_2 surface. Since the motion is already restricted to be on the I_1 surface because of the energy integral; the motion of a star in a potential governed by the two integrals of motion must in fact take place in the intersection of the I_1 and I_2 surface. Again by Liouville's theorem since the f must have the same value everywhere on the surface, then the mathematical expression reduces to the following

$$f(x, y, z, u, v, w) = F(I_1, I_2) \tag{2.7}$$

In the case of the Milky way because of the symmetry of the potential the two isolating integrals of motion are the energy and the angular momentum and this reads as

$$f(R, z, u, v, w) = F(E, h) \tag{2.8}$$

where E is the energy and h, the angular momentum. The general idea is to construct self-consistent models for galaxy disc-bulge-halo systems using these DFs. Our aim is to understand the dark matter problem based on all the above concepts. Using the rotational curve as an observational constraint we have developed a model to help us understand better the properties of the dark matter particles. In particular, we wish to determine the value of the velocity dispersion which is an essential input to the experiments that aim at real time detection of dark matter particles. The most popular models that have proved effective are the King's DFs which is a function of only the energy and the Evans' model [10] which is a function of both the energy and the angular momentum. We shall discuss the models based on these DFs, later in this chapter.

2.3 Motivation

Observational evidence for the existence of dark matter (DM) exists now on a wide variety of astronomical length scales starting from the solar system to large clusters of galaxies [11]. The nature and distribution of DM in the Universe are, however, unknown. It is now well recognized that a substantial fraction of the DM on galactic and larger scales must be non-baryonic [12], the most popular candidate being the MACHOS [13].

Currently, a great deal of experimental effort is underway in trying to directly detect the weakly interacting massive DM particles in the laboratory. The experiments are aimed at observing the effects of the impact of mainly the more massive candidate DM particles of

typical mass $\gtrsim$ few GeV with targets maintained at cryogenic temperatures which facilitate the observation of tiny amount of energy deposited in the process against the background generated by internal and external radioactivity and by cosmic rays. These developments are reviewed in detail by a number of authors [14, 15].

The interpretation of these experiments to derive constraints on the properties of the unknown particles constituting a halo of DM in and around the Galaxy requires assumptions about the density and spectrum of velocities of the DM particles in the solar neighbourhood. These parameters have been obtained thus far by describing the DM halo as a single-component isothermal sphere appropriately truncated at a particular radius [16]. The mass density contributed by DM particles in the solar neighbourhood is not known and is model dependent; however, an analysis of the observed spatial and velocity distribution of the stars near the solar system,as discussed in Chapter 1, indicates a DM density of $\approx 0.3\,\mathrm{GeVcm^{-3}}$ in the solar neighbourhood. In contrast, determination of the 3-D dispersion velocity of the DM particles, $\langle v^2\rangle_{\rm DM}^{1/2}$, has received very little attention. It is customary, to invoke a relation [17] pertaining to a single-component isothermal sphere, and setting $\langle v^2\rangle_{\rm DM}^{1/2} = \sqrt{\frac{3}{2}}V_{c,\infty}$, where $V_{c,\infty}$ is the asymptotic value of the rotation speed V_c, of the Galaxy. Since the value of $V_{c,\infty}$ for the Galaxy is not known and cannot be determined, the usual practice is to *assume* that the rotation curve of the Galaxy [18, 19], $V_c(R)$, as a function of the Galactocentric distance R in the plane of the Galaxy, is flat for all $R \sim 5\,\mathrm{kpc}$ out to $R \gg R_\odot \approx 8.5\,\mathrm{kpc}$ (here $R_\odot$ denotes the position of the solar system), and set $V_{c,\infty} \approx V_c(R_\odot) \approx 220\ \mathrm{kms^{-1}}$, the rotation speed near the solar system. This yields $\langle v^2\rangle_{\rm DM}^{1/2} \approx 270\ \mathrm{kms^{-1}}$, which is the value usually assumed for $\langle v^2\rangle_{\rm DM}^{1/2}$ in most studies of issues related to Galactic DM.

There are, however, reasons to question the above 'determination' of the value of $\langle v^2\rangle_{\rm DM}^{1/2}$. Firstly, the single-component isothermal sphere, without adding the effects of the visible matter, of the Galaxy with $R_\odot$ provides a poor description of the dynamics of the Galaxy in and near the Solar system: The density of the visible matter in the central region of the Galaxy exceeds that of the DM by factors of ~ 1000. Even the integrated mass of the DM within a sphere of radius $R_\odot \sim 8.5\,\mathrm{kpc}$ is smaller than that of the visible matter. In other words, the DM is not the dominant component of matter within the solar circle. Thus the above mentioned asymptotic relation between V_c and $\langle v^2\rangle_{\rm DM}^{1/2}$ can be expected to be valid only at $R \gg R_\odot$ where the DM component described by an isothermal sphere may be expected to be dominant, and not at $R \sim R_\odot$. Moreover, since the basic equation which determines the potential and the density distribution of dark matter depends nonlinearly on the potential exerted by visible matter, inclusion of this additional visible component in the equation

substantially changes the distribution of dark matter. Secondly, there is no observational support for the common assumption that the Galactic rotation curve is already saturated at its asymptotic value at $R = R_\odot$. In fact, as noted by Fich and Tremaine [4], much of the data indicates that the rotation curve "continues to rise" beyond $R_\odot$. Thus even if one assumes the validity of the single-component isothermal sphere description of the Galaxy, the estimate $\langle v^2 \rangle_{\rm DM}^{1/2} \approx 270$ kms^{-1}obtained by assuming $V_c(R_\odot) = V_{c,\infty}$ is uncertain. Thirdly, it is not serious for the problem at hand, it may be noted that the assumption of a pure isothermal *sphere* for the description of the DM halo neglects the deviation from spherical symmetry induced by the disk-like distribution of the visible matter. Keeping these points in mind, we have developed a formalism in which we directly address the question of the phase-space structure of the distribution of DM in the Galaxy, and determine $\langle v^2 \rangle_{\rm DM}^{1/2}$, which enters as a free parameter in this phase-space description, by comparing the theoretical rotation curve with the observed data. Our model of the Galaxy comprises of visible matter and particles of DM coupled through their mutual gravitational potentials in a *self-consistent* manner. This necessarily makes the relevant coupled Poisson and collisionless Boltzmann system of equations for the DM depend non-linearly on the potential generated by the visible matter of the Galaxy non-linear. We solve this non-linear system of equations by means of a simple iterative scheme. In our analysis the departure from spherical symmetry of the halo emerges naturally due to the disk like distribution of the visible matter which we take to be axially symmetric. In this chapter, we discuss our formalism in detail, including a detailed discussion of our numerical algorithm and present several new results. We find that a relatively high value of $\langle v^2 \rangle_{\rm DM}^{1/2} \sim 600$ kms^{-1}(as compared to the earlier expectations of ~ 270 kms^{-1}) is required in order to fit the rotation curve data of the Galaxy.

Further confirmation of the robustness of our result is obtained by performing the calculation for a somewhat more realistic phase-space distribution function for the DM halo, namely the one describing a truncated isothermal sphere, or the so-called "King model". for the on-going laboratory experiments in search of the DM particles. From theoretical point of view, the relatively high dispersion velocity of the DM particles seems to fit in more easily with the 'embedding' scenario [20] according to which galaxies are embedded in cluster-size 'clouds' of DM, rather than with the conventional scenario in which individual galaxies are surrounded by individual 'halos' of sizes much smaller than those of typical clusters.

2.4 Formalism

The phase-space distribution function (DF) of the DM particles, $f_{\rm DM}(\mathbf{x},\mathbf{v})$, satisfies the collisionless Boltzmann equation (see, e.g., Binney and Tremaine 1987). In steady state, the well-known Jeans theorem [17] allows the DF to be expressed as a function of the various integrals of motion of the system. The simplest *ansatz* for $f_{\rm DM}(\mathbf{x},\mathbf{v})$ is obtained by taking it to be a dimensionless function of the energy $E = m\left(\frac{1}{2}v^2 + \Phi_{\rm vis}(\mathbf{x}) + \Phi_{\rm DM}(\mathbf{x})\right)$, where m and v are the mass and velocity of a DM particle, respectively, and $\Phi_{\rm vis}(\mathbf{x})$ and $\Phi_{\rm DM}(\mathbf{x})$ are the gravitational potential due to visible and dark matter, respectively, at the coordinate location x. To illustrate our method, we consider as an example the simplest and most well-known of such a DF, namely the "Maxwellian" describing an isothermal gravitating sphere (see, e.g., Binney and Tremaine 1987):

$$f_{\rm DM}(\mathbf{x},\mathbf{v}) \propto \exp\left[-\frac{E}{k_{\rm B}T_{\rm DM}}\right] \tag{2.9}$$

where the 'temperature' $T_{\rm DM}$ is related to $\langle v^2\rangle_{\rm DM}^{1/2}$, the three-dimensional isotropic velocity dispersion of the DM particles, through the relation $\frac{3}{2}kT_{\rm DM} = \frac{1}{2}m\langle v^2\rangle_{\rm DM}$, and $k_{\rm B}$ is the Boltzmann constant. This DF, as well as the "King model" DF described in the next section, are specially suited for our purpose because they incorporate the crucial quantity of our interest, namely, $\langle v^2\rangle_{\rm DM}^{1/2}$, directly in the DF, allowing us to directly probe the sensitivity of a measurable quantity such as the Galactic rotation speed to variations in $\langle v^2\rangle_{\rm DM}^{1/2}$, and thereby to determine its value.

Now, integrating Eq [2.9] over velocity we can write the DM density, $\rho_{\rm DM}(\mathbf{x})$, as

$$\rho_{\rm DM}(R,z) = \rho_{\rm DM}(0,0)\exp\left[-\frac{3}{\langle v^2\rangle_{\rm DM}}\left\{\left(\Phi_{\rm DM}(R,z) - \Phi_{\rm DM}(0,0)\right) + \left(\Phi_{\rm vis}(R,z) - \Phi_{\rm vis}(0,0)\right)\right\}\right] \tag{2.10}$$

where $\Phi_{\rm vis}(R,z)$ is the visible matter potential at any given point (R,z); Eq [2.10] is normalised with respect to the dark matter and visible potential at the centre. where we have explicitly indicated the density and the potentials as functions of cylindrical polar coordinates, $R = (x^2+y^2)^{\frac{1}{2}}$ and z, in anticipation of the axial symmetry in the problem introduced by the axially symmetric distribution of the visible matter considered in the next section.

The DM potential satisfies the Poisson equation,

$$\nabla^2\Phi_{\rm DM}(R,z) = 4\pi {\rm G}\,\rho_{\rm DM}(R,z) \tag{2.11}$$

Now, for a *given* visible matter potential, $\Phi_{\rm vis}(R,z)$, as constructed from a suitable representation of the observed mass density distribution of the visible matter in the Galaxy, the exercise

is to obtain the DM potential $\Phi_{\rm DM}(R,z)$ by *self-consistently* solving the coupled non-linear equations (2.11) and (2.10). In this exercise, the central density of the DM halo, $\rho_{\rm DM}(0,0)$, and the DM velocity dispersion, $\langle v^2\rangle^{1/2}_{\rm DM}$, appear as free parameters which are determined by directly fitting the rotation speed of the Galaxy calculated from the expression

$$V_c^2(R) = R\frac{\partial}{\partial R}\Big[\Phi_{\rm DM}(R,z) + \Phi_{\rm vis}(R,z)\Big]_{z=0} \tag{2.12}$$

to the observed rotation speed data.

The solution of the coupled equations (2.10) and (2.11) for $\Phi_{\rm DM}$ is effected through the following iterative scheme: In the zeroth order, we set the DM potential to zero in Eq [2.10]. Since $\Phi_{\rm vis}$ is known, this gives us the zeroth order approximation for $\rho_{\rm DM}$, which when substituted on the right hand side of Eq [2.11], allows us to solve Eq [2.11] to obtain the 1st-order approximation for $\Phi_{\rm DM}$. The latter is then used in Eq [2.10] and the resulting $\rho_{\rm DM}$ substituted in Eq [2.11] to obtain the 2-nd order approximation for $\Phi_{\rm DM}$, and so on. In compact notation, this iteration scheme can be expressed as

$$\nabla^2\Phi_n(R,z) = 4\pi G\rho_{n-1}(R,z) \tag{2.13}$$

where $n = 1,2,3,\ldots$, and $\rho_{n-1}(R,z)$ is equal to the right hand side of Eq [2.10] with $\Phi_{\rm DM}$ replaced by Φ_{n-1}. The iteration is set off by taking, for $n = 0$, $\Phi_0(R,z) = \Phi_0(0,0) = 0$. It turns out that this is a simple and a very efficient iteration scheme, and we find that the potentials Φ_n's converge towards the desired potential $\Phi_{\rm DM}$ typically within a few iterations ($n \lesssim 10$). Details of the actual numerical algorithm including implementation of the relevant boundary conditions and the tests for checking the correctness of the numerical code are described later.

2.5 Models for Dark and Visible Matter

(i) The phase-space distribution function for Dark Matter

As explained in the previous section, since we are interested in the velocity dispersion of the DM particles, a model for the DM must be prescribed at the level of the phase space DF, and not just at the level of mass distribution. Note that while a given phase space DF leads to a unique mass distribution, the converse is not true in general. The DF describing the Galactic DM is not known *a priori*. The Maxwellian DF describing an isothermal gravitating sphere discussed in the previous section is widely used in the literature in this context. In this

chapter, we consider, in addition to the Maxwellian model, the so-called "lowered isothermal" or "King model" [17] DF given by

$$f(\mathcal{E}) = \begin{cases} \rho_1 (2\pi\sigma^2)^{-\frac{3}{2}} (e^{\mathcal{E}/\sigma^2} - 1) & \mathcal{E} > 0 \\ 0 & \mathcal{E} \leq 0 \end{cases} \tag{2.14}$$

where $\mathcal{E}$ is the so-called "relative energy" [17] defined as $\mathcal{E} \equiv -E + \Phi_0$, where Φ_0 is a constant, and ρ_1 and σ are the density and velocity parameters of the model. In practice, the constant Φ_0 is chosen such that $f > 0$ for all $\mathcal{E} > 0$ and $f = 0$ for all $\mathcal{E} \leq 0$. Unlike the case of the Maxwellian DF of Eq [2.9], the velocity dispersion in the King model is not spatially constant. Indeed, the King model DF, by construction, has the property that the mass density as well as the velocity dispersion vanish at a finite distance from the center, called the "tidal radius", r_t, which is a free parameter of the model. In contrast, recall that the Maxwellian isothermal sphere is 'infinite' in extent; its mass density has the asymptotic ($r \to \infty$) behavior $\rho(r) \propto r^{-2}$, where r is the radial distance. For a DM halo described by the King model, the DM velocity dispersion $\langle v^2 \rangle_{\rm DM}^{1/2}$ decreases [17] slowly from $\sqrt{3\sigma^2}$ at $r = 0$ to zero at $r = r_t$. Because of these properties, the King model is expected to provide perhaps a more 'realistic' description of a finite DM halo than the 'infinite' Maxwellian isothermal model. However, in practice, we find that the Galactic rotation curves calculated by using the above two DFs differ significantly from each other only at distances $R > 30\,\mathrm{kpc}$ for typical values of $r_t \approx 300\,\mathrm{kpc}$. Since reliable rotation speed data for the Galaxy exist only for distances $R \lesssim 20\,\mathrm{kpc}$, and since we are interested in the value of $\langle v^2 \rangle_{\rm DM}^{1/2}$ at $R \sim R_\odot \approx 8.5\,\mathrm{kpc}$, the difference in the rotation curves of the two models at $R > 30\,\mathrm{kpc}$ does not influence our results significantly so that both DFs yield roughly the same value of $\langle v^2 \rangle_{\rm DM}^{1/2}$ in the solar neighbourhood as determined by comparing the predicted rotation curves to the observed data.

Clearly, the exact DF describing the DM halo of the Galaxy is unknown. The two 'thermal' DFs mentioned above are used in our analysis primarily from the point of view of simplicity. Other DFs for the DM have been advocated in the literature [10]. There is some theoretical justification, however, for using the 'thermal' DFs: the origin of the DM particles in the early Universe would be expected to start their DF off with a thermal distribution which may have been marginally affected by violent relaxation and coarse graining during the growth of the structures in the Universe. In any case, we expect that the estimate of $\langle v^2 \rangle_{\rm DM}^{1/2}$ obtained by using the rotation curve as a probe would be weakly sensitive to the exact form of the DF used in the analysis. This can be understood as follows: in the absence of streaming flow (i.e., $\langle v \rangle = 0$), the leading moment $\langle v^2 \rangle$ determines the "pressure" term in the Jeans

equations (see Eq (4-27) of [17] and the discussions following it). Thus for all pressure-supported DM halo models the values of $\langle v^2 \rangle_{\rm DM}^{1/2}$ determined by a given set of rotation speed data would be expected to be roughly the same. The central density of the DM halo is also determined in our analysis and is also being independently constrained by the Oort-Bahcall type estimates [21, 22, 14, 24] of the DM density in the solar neighbourhood.

(ii) Model for the visible matter

We now have to specify the density distribution of the visible matter and the resulting gravitational potential used in the analysis. We use a two-component model of the visible matter consisting of a spheroidal bulge [17, 25, 26] with density $\rho_s(r)$, and an axisymmetric disk [26] with density $\rho_d(R,z)$:

$$\rho_s(r) = \frac{\rho_0}{(1+r^2/a^2)^{3/2}} \tag{2.15}$$

$$\rho_d(R,z) = \frac{\Sigma_\odot}{2h} e^{-(R-R_\odot)/R_d}\, e^{-|z|/h}, \tag{2.16}$$

where $r = (R^2+z^2)^{1/2}$, and disk surface density at the solar position, z being the vertical distance from the plane of the disk. The values of the parameters are given by $a = 0.103\,\mathrm{kpc}$, $R_d = 3.5\,\mathrm{kpc}$, $h = 0.3\,\mathrm{kpc}$, and $\rho_s(R_\odot) = 7 \times 10^{-4} M_\odot pc^{-3}$ [25, 26]. It may be mentioned here that the rotation curve in the outer regions of the Galaxy is relatively insensitive to the spheroid parameters. There are large discrepancies in the values of $\Sigma_\odot$ reported in the literature: Whereas Kuijken and Gilmore (KG) [26] suggest $\Sigma_\odot \sim 40 M_\odot pc^{-2}$ on the basis of analysis of a sample of data on ~ 512 K-dwarf stars, Bahcall *et al.* [14, 24] in their reanalysis of essentially the same data suggest a number for $\Sigma_\odot$ which is about twice as large. The estimate of the local surface density of the Galactic disk due to the identified matter such as visible stars is $\sim 48 \pm 8 M_\odot pc^{-2}$. Thus Bahcall *et al.* 's kinematical estimate of $\Sigma_\odot$ seems to indicate the presence of a substantial amount of unseen matter associated with the disk, whereas KG's estimate is consistent with no disk dark matter. In this context, it is perhaps worthwhile to mention that the analyses of Refs. [14, 24, 26] are all based on one-dimensional solutions to the Boltzmann equation which are strictly valid for an infinite disk only. In any case, the dark matter associated with the disk is expected to be dissipational in contrast to the collisionless and non-dissipative dark matter constituting the extended halo of the Galaxy We shall, therefore, use the conventional nomenclature "visible" to describe effectively the *total* (i.e., visible plus dark) matter associated with the disk. The value of $\Sigma_\odot$ is a source of

uncertainty in our estimated value of $\langle v^2 \rangle_{\rm DM}^{1/2}$. In our calculations, we shall consider values of $\Sigma_\odot$ in the range $40 - 80 M_\odot pc^{-2}$. Note, however, that the contribution of the disk to $V_c^2(R)$ defined in Eq [2.12] is proportional to its surface density, while that of a perfect isothermal sphere is proportional to the square of the velocity dispersion of its constituent particles (see Eqs(4-159) and (4-127b) of Ref. [17]). Thus, for a given observed rotation curve, the use of higher values of $\Sigma_\odot$ in the calculation is expected to yield correspondingly lower values of $\langle v^2 \rangle_{\rm DM}^{1/2}$ as obtained by comparing the predicted and observed rotation curves. This expectation is indeed borne out by our numerical calculations giving a *lower limit* to the estimated value of $\langle v^2 \rangle_{\rm DM}^{1/2}$ corresponding to $\Sigma_\odot \sim 80 M_\odot pc^{-2}$.

2.6 Numerical Procedure

In this section we describe the algorithm we have used for solving the coupled non-linear partial differential equation (PDE) Eq [2.11] for the dark matter potential. The coupled non-linear equation along with the boundary conditions is described below.

$$\frac{1}{r^2}\frac{\partial}{\partial r}\left(r^2\frac{\partial \Phi}{\partial r}\right) + \frac{1}{r^2 \sin\theta}\frac{\partial}{\partial \theta}\left(\sin\theta \frac{\partial \Phi}{\partial \theta}\right) = 4\pi G\rho \tag{2.17}$$

$$\left.\frac{\partial \Phi}{\partial r}\right|_{r=0} = 0, \qquad \left.\frac{\partial \Phi}{\partial r}\right|_{r=rmax} = \frac{GM(r)}{r^2} \tag{2.18}$$

$$\left.\frac{\partial \Phi}{\partial \theta}\right|_{\theta=0} = 0, \qquad \left.\frac{\partial \Phi}{\partial \theta}\right|_{\theta=\pi} = 0$$

At large distances corresponding to $r = rmax$ the dark matter distribution is spherically symmetric. The force at the center of the Galaxy will be zero purely by symmetry arguments and the normalization is chosen such that the potential at the center is always zero. Only the radial component of force is present at large distances and is a function of the mass enclosed at that radius.

The polar coordinate system would be the most natural one to solve this problem. However to simplify the problem numerically we have used the following transformation which maps a polar coordinate system almost to the Cartesian coordinate system with exception of the point at the origin. The transformation is given by $x = \ln(r)$ and $y = \theta$.

We use a two-fold iterative procedure to solve this equation. In principle the non-linear

elliptic equation we have to solve is of the form:

$$\nabla^2 u = f(u) \tag{2.19}$$

where $f(u)$ is some function, in the problem at hand it is the density. We specify an initial value to u^0 such that $f(u)$ is completely defined. Then the equation reduces to a linear elliptic function which is solved using the successive- over- relaxation method. The new converged value of u^1 is again used to compute the new $f(u)$ and the linearlised equation solved to obtain another u^2. This process is continued till a converged value of u^n is obtained.

As a first step we discretise the equations using the finite difference scheme. Eq [2.17] can be rewritten in the discretised version, after making the transformation to the (x,y) coordinate system described above, as

$$f(i,j) = a(i,j)u(i+1,j) + b(i,j)u(i-1,j) + c(i,j)u(i,j+1) + d(i,j)u(i,j-1) + e(i,j)u(i,j) \tag{2.20}$$

$$\begin{aligned}
a(i,j) &= dy^2(2+dx) \\
b(i,j) &= dy^2(2-dx) \\
d(i,j) &= dx^2\left(\frac{dy}{\tan(y(j))}+2\right) \\
c(i,j) &= dx^2\left(2-\frac{dy}{\tan(y(j))}\right) \\
e(i,j) &= -4(dy^2+dx^2) \\
f(i,j) &= 8\pi\rho(i,j)e^{2x}dx^2dy^2
\end{aligned}$$

where $u(i,j)$ is the discretised potential at the coordinate x_i and y_j; dx and dy are the grid sizes for a rectangular grid of 701 × 61. The discretised density, $\rho(i,j)$ with the two parameters: the central density $\rho_{\rm DM}(0)$ and the velocity dispersion $\langle v^2\rangle^{1/2}_{\rm DM}$ is given by

$$\rho(i,j) = \rho_{\rm DM}(0)\exp\left[-\frac{3}{\langle v^2\rangle^{1/2}_{\rm DM}}\Big(u(i,j)+u_{\rm vis}(i,j)\Big)\right] \tag{2.21}$$

The discretised version of the equation to be solved is for $u(i,j)$ (Eq [2.20]).

$$\begin{aligned}
u^{n+1}(i,j) &= \frac{1}{e(i,j)}\Big(f(i,j) - a(i,j)u^n(i+1,j) - b(i,j)u^n(i-1,j) \\
&\quad + c(i,j)u^n(i,j+1) + d(i,j)u^n(i,j-1)\Big)
\end{aligned} \tag{2.22}$$

There are two sets of iterations involved in solving this non-linear PDE, as described earlier. At every step of n, the linearised equation has to be solved iteratively. We specify the initial

values for the $u^0(i,j)$ so that the density $\rho(i,j)$ in Eq [2.21] is fully specified and $f(i,j)$ has no explicit dependence on $u(i,j)$. This linear equation is then solved using the relaxation scheme [27] to determine the new $u^1(i,j)$ (Eq [2.23]). The converged new solution is used to determine the new $f(i,j)$, which again reduces the Eq [2.23] to a linearised equation which is solved by the usual relaxation method mentioned earlier. Thus the outer iteration consists of finding new values for $f(i,j)$ and the inner iteration is used to determine the converged $u^{n+1}(i,j)$. The outer iterations are continued till a converged value for $u^n(i,j)$ is obtained. Typically 10 outer iterations and 30000 inner iterations are required to solve this equation We have checked for convergence both in the inner iteration and the outer iteration and the convergence is of the order of 10^{-4}. Using this numerical procedure we obtain

$$\langle v^2 \rangle_{\rm DM}^{1/2} = 600 \text{ kms}^{-1}$$

(i) Checks and Comparisons

We have checked the validity of the numerical algorithm we have developed. Here we demonstrate the various tests we have performed on the code to ensure its robustness and hence the value of the velocity dispersion. Following the earlier paper our numerical results were further confirmed by Bienayme *et al.* [28].

First, since at each step of the outer iteration one is actually solving the Poisson equation with the source term known, we checked the Poisson solver itself for the Miyamoto-Nagai potential. To test the code we also solved it without the theta dependence retaining only the radial component whose analytical solutions are well known [17]. The analytical and numerical results compare to better than 1% accuracy. At large distances, the dark matter is the dominant component; from Eq [2.21] we note that the equation reduces to that of an isothermal sphere for $u_{\rm vis} \approx 0$. Therefore, in this limit the algorithm should reproduce all the behavior pertaining to that of an isothermal sphere. For an isothermal sphere we know that the rotation curve asymptotically approaches a flat rotation curve with the value given by the equation $V_c(R) = \frac{3}{2}\langle v^2 \rangle_{\rm DM}$. Hence, for $\langle v^2 \rangle_{\rm DM}^{1/2} = 600 \text{kms}^{-1}$ this reduces to the expected value of 490 kms^{-1} for the rotation speed V_c. This is clearly demonstrated in the Fig [2.1] below. We have also calculated the slope of the density ($\rho \sim r^{-2}$) and as seen from the Fig [2.1], it approaches the expected value of 2.

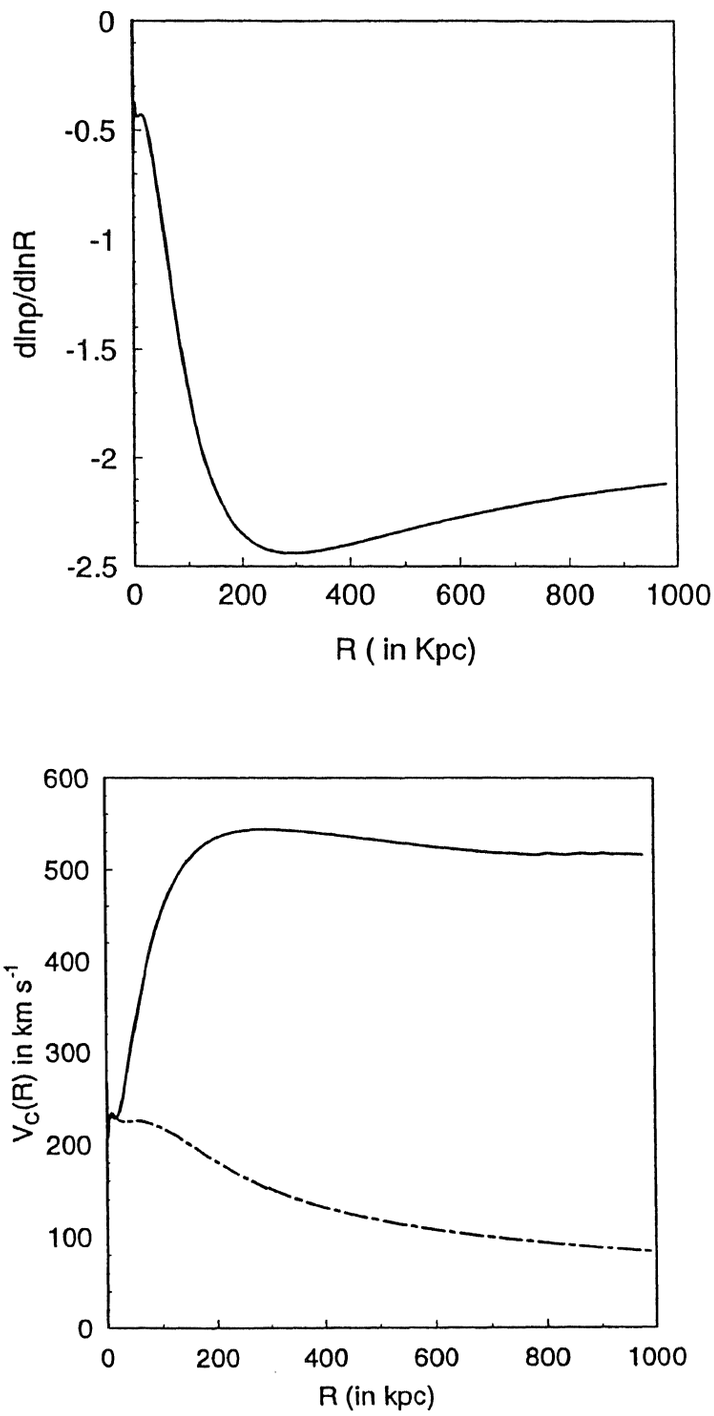

Figure 2.1: The figure on the top demonstrates that $\rho \approx r^{-2}$. The figure below shows that the rotation curve approaches a flat curve at large distances. Note that for a velocity dispersion of 600 kms^{-1}(solid line) the V_c approaches 490 kms^{-1}as expected from the relation $V_c^2(R) = \frac{3}{2}\langle v^2 \rangle_{DM}$.

2.7 Results

Having obtained the potential of the dark matter for the Galaxy we proceed to derive the rotation curve. The rotation speed is given by

$$V_c(R) = R\frac{\partial}{\partial R}(\Phi_{vis} + \Phi_{DM}) \tag{2.23}$$

The Fig [2.2] shows the rotation curve calculated for various values of the $\langle v^2\rangle_{DM}^{1/2}$. The data are taken from various sources, at small distances $0-2$ kpc from Burton & Gordon [29] and at large distances from Fich *et al.* [4], the current data on the Galaxy are available up to 20 kpc. In order to determine the best-fit value we have calculated

$$\chi^2 = \frac{1}{N}\sum_{i=1}^{N}\left(\frac{V_i(R_i) - V_{i,\sigma}}{\sigma_i}\right)^2$$

as a function of $\langle v^2\rangle_{DM}$ where N is the number of observational data points , $V_i(R_i)$ and $V_{i,\sigma}$ are the theoretical and observational values for the rotation speed respectively for the i^{th} data point for which $R = R_i$ and σ_i is the 1σ uncertainty in the measured value for $V_{i,\sigma}(R_i)$.

The chi-square (Fig [2.2]) is plotted as a function of $\langle v^2\rangle_{DM}$ and it clearly follows that the $\langle v^2\rangle_{DM}^{1/2}$ of the order of 600 kms^{-1}. *Our results are based on the best available rotation curve data upto* 20 kpc *and do not rely on extrapolation of the data beyond the last observed point.* The expected asymptote is approached at large distances for the various values of velocity dispersion.

We have carried out the above analysis for different values of $\rho_{DM}(0)$ ranging from 0.3 GeVcm^{-3} to 1 GeVcm^{-3} for different values of the velocity dispersion. We believe this is an independent way of estimating the density of the dark matter from the rotation curve.

Also as mentioned previously we have carried out the analysis with the King's model which has a cut off at a finite radius. We have derived the rotation curve based on this model and made estimates on the the $\langle v^2\rangle_{DM}^{1/2}$ of the dark matter particles. Interestingly we find that we obtain approximately the same value for $\langle v^2\rangle_{DM}^{1/2}$, *i.e.*, 570 kms^{-1} (Fig [2.3]) as the best fit value. The velocity dispersion, in general is calculated as:

$$\langle v^2\rangle_{DM} = \int_0^\infty f(E)v^2 d^3v \tag{2.24}$$

In the case where $f(E)$ is the isothermal model, the $\langle v^2\rangle_{DM}^{1/2} = 3\sigma^2$ and is a constant; however using the King's model one obtains the velocity dispersion as a function of the distance which is shown in Fig [2.4]. Thus the determination of the velocity disperison of dark matter

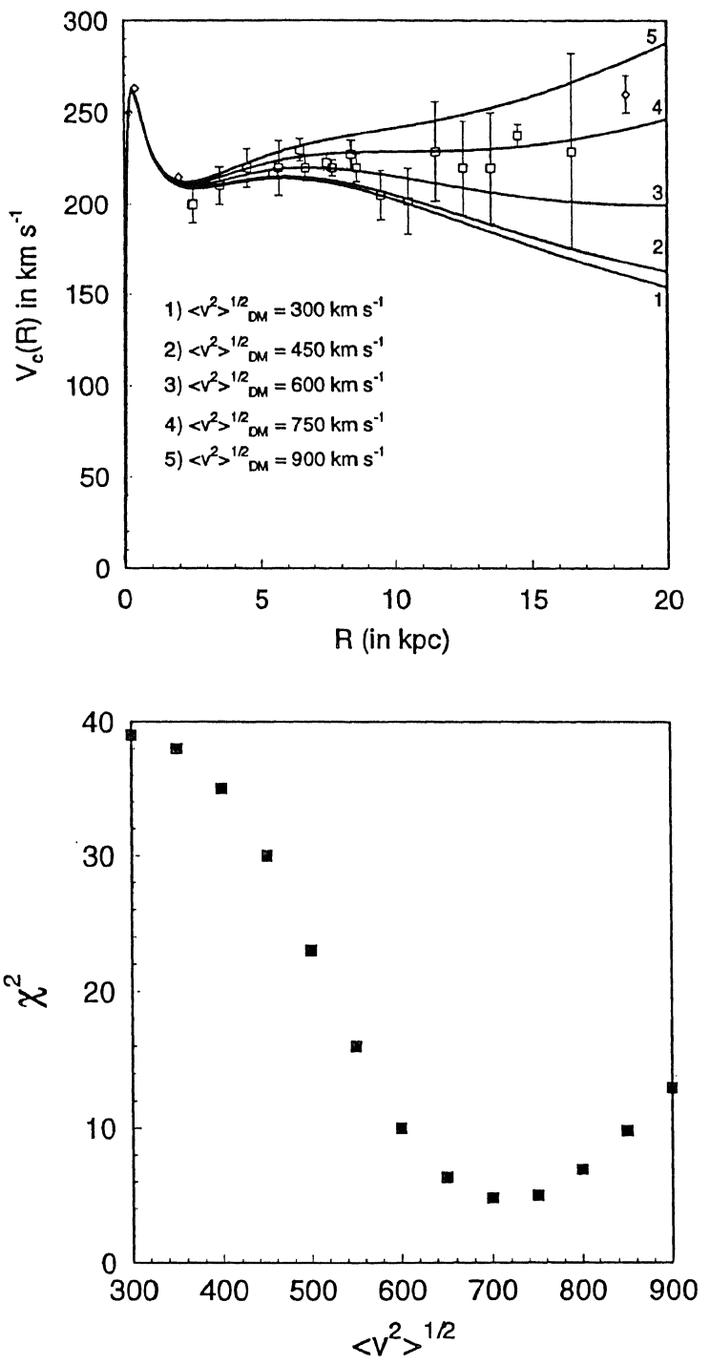

Figure 2.2: The theoretically estimated rotation curve compared with the observations of Fich *et al.* is shown in the first figure. The second figure plots the chi-square value for different values of the $\langle v^2\rangle^{1/2}_{DM}$ obtained by comparing the theoretical and observed rotation curves.

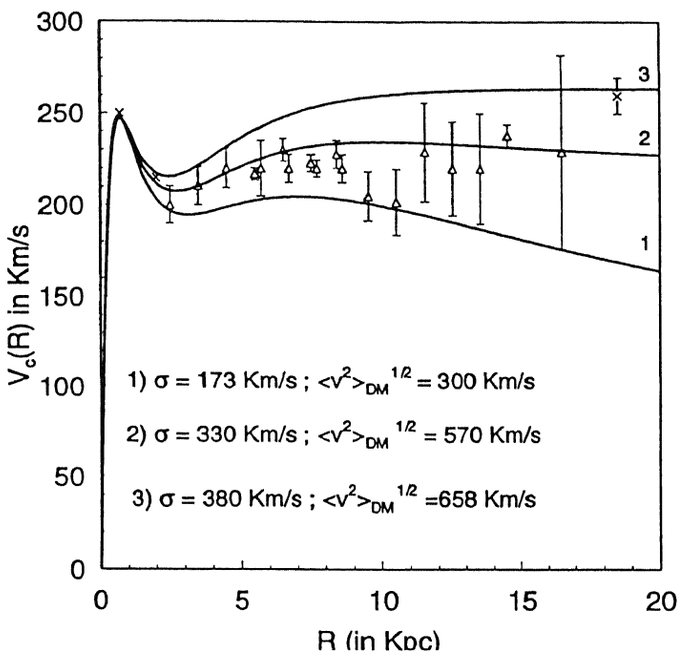

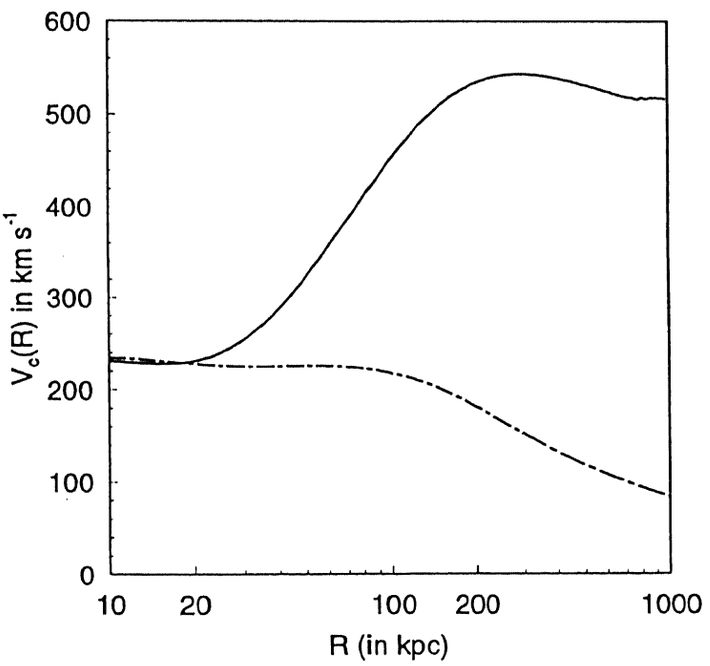

Figure 2.3: In the first figure we show the rotation curve fit, using the King's model, with the observed data. The best fit value is obtained for $\langle v^2 \rangle_{DM}^{1/2} = 570$ kms^{-1}. The second figure compares the rotation curve due to the isothermal and King's models. It is clear that at small distances both models show similar behaviour of rotation curve.

particles from the rotation curve appears to depend rather weakly on the assumed form of DF. In the Fig [2.3] we have shown the rotation curve derived using both the King's model and the isothermal model superposed on each other. It is very clear that at small distances the two models are very similar in behavior and its not surprising that the $\langle v^2 \rangle_{\rm DM}^{1/2}$ has the same value at the Solar neighbourhood.

2.8 Discussion

We have used a two component model to describe the galaxy; the visible and dark matter components. This implies that at distances where the visible matter is dominant it modifies the parameters of the dark matter distribution as we have seen in the case of $\langle v^2 \rangle_{\rm DM}^{1/2}$. Secondly as, we have pointed out earlier the value for the $\langle v^2 \rangle_{\rm DM}^{1/2} \approx 270$ kms^{-1}was derived on the basis of assuming $V_c(R_\odot) = V_{c,\infty}$ and then using the virial relation $\langle v^2 \rangle_{\rm DM} = 2V_c(R_\odot)/3$. The use of this relation in the Solar neighbourhood region definitely has neither basis nor justification. For, this relation is valid for a single component of the isothermal sphere and the rotation curve is flat from $R = 8.5\,$kpc.

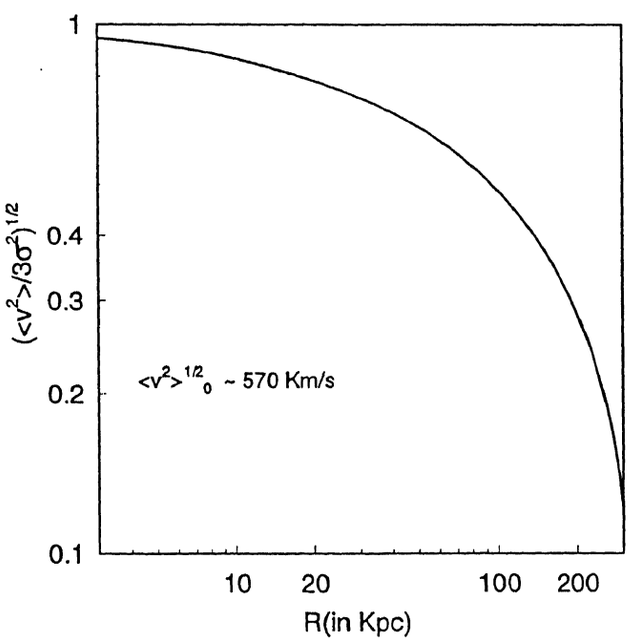

Figure 2.4: The variation of the velocity dispersion as a function of galactocentric radius.

In fact, the Fich *et al.* [4] data indicates that there is a rising rotation curve. It is true the rotation curve rises rather sharply for the isothermal model and then saturates at the expected value according to the virial theorem (for a $\langle v^2 \rangle_{DM} \approx 600$ kms^{-1}it saturates at $V_c \approx 490$ kms^{-1}). Since there is an uncertainty of a factor of two in the value of the $\rho_{DM}(R_\odot)$, we have taken a range of parameter values of $\rho_{DM}(0)$ (central density) varying from $0.3 - 10\,\mathrm{GeVcm}^{-3}$ for the various $\langle v^2 \rangle_{DM}$. Thus we have tried to scan, as much as possible the parameter space of ρ and $\langle v^2 \rangle_{DM}$. Thus in some sense this work also tries to place an independent constraint on the $\rho_{DM}(0)$. One of the consequences of assuming a Maxwellian distribution is that the velocity dispersion is a constant . If one assumes a different phase space distribution like that of a truncated isothermal sphere, it is true that the $\langle v^2 \rangle_{DM}$ is a function of R; however as explained earlier, since this is only the second moment of the distribution function it really does not matter what distribution one chooses at small distances since it is only the large distance behavior that is very different.

There are 6 observational variables $(\vec{r}\ ,\vec{v})$ for each of the objects on which the observations focus and a large statistical sample is necessary to get a model for the mass distribution. Unfortunately, it has thus far been possible to observe only 4 variables $\vec{r}$ and v_{radial}, leaving the models highly under constrained thus requiring specific assumptions about the model. The work by Norris and Hawkins, Frenk and White *et al.* [12] addresses the question of mass models and not the phase space structure of the Galaxy. Moreover the circular speeds derived with their mass models [12] are not inconsistent with the ones we have derived here. As noted in our letter [18, 32, 33, 34] we have done the calculation with the truncated isothermal model and found that the value for the velocity dispersion is not inconsistent with what we have for the isothermal model.

As Bienayme *et al.* [28] further pointed out, this calculation has to be extended further by applying the model to 6D data from globular clusters and obtaining a realistic upper limit on the $\langle v^2 \rangle_{DM}^{1/2}$. It is also necessary now to check for consistency of this model within the frame work of the local group of galaxies.

(i) Rotating halo models

Thus far our focus has been on non-rotating halos and in this section we discuss some aspects of rotating systems. Rotation gives rise to centrifugal force $\approx rw^2$ which depends quadratically on the angular velocity and increases linearly with distance. The effect of this is to make equipotential spheroids that extend in the equatorial plane. Early work on such halos

were carried out with distribution functions of the form

$$F(E, L_z) \approx \exp[\beta_1 E + \beta_2 L_z^2] \tag{2.25}$$

Such halos had unusual behavior near $r = 0$ for certain values of the parameters β_1 and β_2. Recently Evans suggested the form

$$F(E, L_z^2) = (AL_z^2 + B)\exp(4E/v_0^2) + C\exp(2E/v_0^2) \tag{2.26}$$

with

$$\begin{aligned} A &= \left(\frac{2}{\pi}\right)^{5/2} \frac{(1-q^2)}{Gq^2 v_0^3}, \\ B &= \left(\frac{2}{\pi^5}\right)^{1/2} \frac{R_c^2}{Gq^2 v_0} \\ C &= \frac{2q^2 - 1}{4\pi G q^2 v_0} \end{aligned} \tag{2.27}$$

where R_c is the core radius, q is the flattening parameter and v_0 is some velocity scale in the problem. This DF has more regular features suitable for the description of astrophysical halos. Irrespective of the precise form of the DF in halos with rotation, the centrifugal force adds to the forces generated by the gradient in pressure in supporting the halo against gravitation. In the present context of the study of Galactic dark matter Kamionkowski & Kinkhabhwala, [35] have used the Evans model Eq [2.26] to compute the features of the rotation halos. Their work is similar to the early work on isothermal halos and shows that introducing reasonable amount of rotation does not cause major changes with respect to the behavior exhibited by the isothermal non-rotating systems. In particular, once the asymptotic value of the circular velocity V_c is induced by such a halo is fixed, the value of the underlying velocity dispersion is similar to that of an isothermal halo with the same V_c.

The rotation curve computed by Kamionkowski and Kinkhabhwala, while in agreement with the observations in the range of $15 - 20\,\mathrm{kpc}$, is in gross disagreement with the observed rotation curve upto 10 kpc. One may think that (by adding the contribution of the observed distribution of visible matter) the theoretical rotation curve may be brought into agreement with the observations. However, to do this the effect of the gravitational potential of visible matter on the halo is to be taken into account. As discussed earlier in this chapter the coupling is non-linear and the density of the halo particles will be enhanced substantially at short galactocentric distances $r < 7\,\mathrm{kpc}$, for the same set of parameters describing the phase space distribution of the halo. Thus single component description for the halo dark matter

distribution in untenable whether the DF be a simple isothermal or a rotating form given by Evans. Kamionkowski & Kinkhabhwala have shown the insensitivity of the parameters to reasonable levels of rotation. We have already shown the insensitivity of our results to specific forms of the DF. Combining these two results it may be safe to conclude that the large value of $\langle v^2 \rangle_{DM}^{1/2}$ derived by us is valid for halos rotating slowly.

In conclusion we would like to state that in the wake of new observations and experiments it has become important today to carefully compute the various dark matter parameters involved. We have devised a new model for the halo and computed the value for the velocity dispersion of the dark matter particles to be 600 kms^{-1}in a self consistent fashion. Our model is consistent with the observed rotation curve upto 20 kpc. We have shown that the computed rotation curve is not very sensitive to the phase space distribution at small distances.

Bibliography

[1] Bosma, A., 1978, Ph.D. Thesis, University of Groningen

[2] Rubin, V.C., Ford, K., & Thonnard, N., 1978, ApJL, 225, L107

[3] Blitz, L., 1994, in *AIP Conference Proceedings, No. 336 on Dark Matter*, eds. Stephen S. Holt & Charles L. Bennett, 101

[4] Fich, M., & Tremaine, S., 1991, ARA&A, 29, 409

[5] Schmidt, M., 1985, *The Milky Way Galaxy, IAU symposium no.106*, eds., Van Woerden *et al.* , 75

[6] Bahcall, J.N., Schmidt, M., & Soneira, R.M., 1982, ApJL, 258, L23

[7] Bahcall, J.N., Schmidt, M., & Soneira, R.M., 1983, ApJ, 265, 730

[8] Albada, T.S.Van., Bahcall, J.N., Begeman, K., & Sancisi, R., 1985, ApJ, 295, 305

[9] Kent, S., 1986, AJ, 91, 1301

[10] Evans, N.W., 1993, MNRAS, 260, 191

[11] Trimble, V., 1987, ARA&A, 25, 425

[12] Jungman, G., *et al.* , 1996, Phys. Reports., 267

[13] Alcock, C., 1996, ApJ, 461, 84

[14] Goodman, M. & Witten, E., 1985, Phys. Rev. D., 31, 3059

[15] Press, W. H. & Spergel, D., ApJ, 296, 663

[16] Flores. R.A., 1988, Phys.Lett.B., 215, 73

[17] Binney and Tremaine, *Galactic Dynamics*, 1986

[18] Rubin, V.C., & Ford.W.K., 1970, ApJ, 159, 379

[19] Rubin, V.C., *et al.* , 1980, ApJ, 238, 471; Rubin,V.C., 1983, in*The Internal Kinematics, and dynamics of Galaxies, IAU Symposium no 100*, eds., Athananassoula, E., Reidel:Dordrecht, 3; Boroson, T. 1981, ApJS, 46, 177

[20] Cowsik, R. & Ghosh, P., 1987, ApJ, 217, 26

[21] Oort, J.H., 1932, BAN, 6, 249

[22] Oort, J.H., 1960, BAN, 15, 45

[23] Bahcall, J.N., 1984a, ApJ, 276, 156

[24] Bahcall, J.N., 1984b, ApJ, 276, 169

[25] Caldwell, J.A.R., & Ostriker, J.P., 1981, ApJ, 219, 18

[26] Kuijken, K., & Gilmore, G., 1989a, MNRAS, 239, 571

[27] Press, W.H., *et al.* , *Numerical Recipes in Fortran*, 1986

[28] Bienayme, O., & Pichon, C., 1997, A&A, L43

[29] Burton, W.B., & Gordon, M.A., 1978. A&A, 63, 7

[30] Frenk, C.S., White, S.D.M., 1980, MNRAS, 193

[31] Cowsik, R., Charu Ratnam., & Bhattacharjee, P., 1996, Phys.Rev.Lett., 76, 3886

[32] Cowsik, R., Charu Ratnam., & Bhattacharjee, P., 1997, Phys.Rev.Lett., 78, 2260

[33] Evans, N.W., 1997, Phys. Rev. Lett., 78, 2261

[34] Gates, E., Kamiokowski, M., & Turner, M.S., 1997, Phys.Rev.Lett., 78, 2262

[35] Kamionkowski, M., & Kinkhabhwala, A., hep-ph/9710337

Chapter 3

Dwarf Spheroidals & Rotation Curves

In an earlier chapter we noted that our conclusions about the velocity dispersion of the DM particles depended on the behaviour of the rotation curve of the Galaxy at large distances. The observations of the rotation curve in the Galaxy are poor beyond the Solar circle and there is no direct information beyond 18 kpc. In this chapter we follow up a suggestion by Lynden-Bell and Lynden-Bell [1] that the motion of dwarf spheroidal galaxies may be used to indirectly derive the rotation curve of the Galaxy up to 200 kpc. In the Section [3.1] we review some of the studies on dwarf spheroidals. Section [3.2] discusses our own work on these galaxies and highlights how it is consistent with the work done in the earlier chapter.

3.1 Review of Dwarf Spheroidal Galaxies

The dwarf spheroidals (DS) are interesting objects of study; they are the smallest known systems only a few hundred parsecs across, in which dark matter has been detected. The DS are small galaxies with a typical mass of $10^6 M_\odot$ and low surface brightness. A dynamical estimate of dark matter is obtained by measuring velocity dispersion of individual stars and applying the virial theorem. Assuming that the light traces the mass distribution and the velocity dispersion is isotropic, the King's model has been used to fit the star counts of the dwarf spheroidals. The King's model yields

$$\rho_0 = \frac{9\sigma_{0p}}{4\pi G r_c^2} \tag{3.1}$$

and

$$\frac{M}{L} = \frac{9\sigma_{0p}}{2\pi G \Sigma_0 r_c} \tag{3.2}$$

where σ_{0p} is the central projected velocity dispersion, Σ_0 the central surface brightness and r_c the core radius. These parameters have associated with them an observational uncertainty. For example, Aaronson [2] reported a velocity dispersion of $\approx$ 10 kms^{-1}for Draco based on measurements of velocities of 3 carbon stars. Pryor *et al.* [3] recently reported observations of velocity dispersions for some DS. These studies indicate that dark matter is present in the dwarf galaxies [4]. In particular, Draco and Ursa Minor seem to have a large central density and a large value for M/L. The DS also have an important role in the dynamical evolution of the Galaxy [5]. These objects are thought among the putative remnants tidally stripped apart from the Galaxy during the earlier stages of galaxy formation [5, 6]. The first suggestion came from Toomre and Toomre [7] who showed that gravitational tides of the Galaxy could result in spectacular features and later the observation of the Large Magellanic Cloud (LMC) suggested the possibility of its tidal origin for remnants in general. The dwarf spheroidals are thought to be debris associated with mergers. There has been a lot of work on DS primarily to obtain the mass of the Galaxy. Lynden-Bell, Canon and Godwin [8] pooled data on these satellite galaxies and obtained a small mass for the Galaxy, of $2 \times 10^{11} M_{\odot}$. This mass was obtained based on the assumption of isotropic orbits for the DS. They argued that tidal disruption would remove preferentially orbits which bring them closer to the Galaxy and they obtained mass atleast 4 times larger by cutting out highly eccentric orbits. Little and Tremaine [9] also assumed isotropic orbits and obtained a small mass for the Galaxy, however they argued against tidal disruption. Their reasoning was based on the fact that since the DS had a large amount of dark matter they had a large mass and are hence stable against tidal disruption. Further studies were carried out by Kulessa and Lynden-Bell [10] with more data including globular clusters the Leo I galaxy which has a large radial velocity. They determined the mass based on a maximum likelihood estimate and also treated the Galactic potential in a self consistent manner to obtain the total mass of the Galaxy as $1.3 \times 10^{12} M_{\odot}$. Cowsik and Ghosh [11] proposed the "embedding model" where the visible galaxies are embedded in a huge dark matter condensate so that light does not trace the mass distribution. They solved the 1-d Poisson equation self consistently for both the stellar and the dark matter distributions and obtained the densities and $\langle v^2 \rangle_{\rm DM}^{1/2}$ by fits to the luminosity profiles. The conclusion they reached was that the luminosity profiles were best fit for a dark matter particle with $\langle v^2 \rangle_{\rm DM}^{1/2} \approx 1000$ kms^{-1}and a background dark matter density of $\rho = 10^{-25} - 10^{-26}$ gm cm^{-3}.

Observations of dwarf spheroidals can also be used to constrain the rotation curve at large galactocentric distances. Based on an analysis by Frenk and Lynden-Bell [12], Lynden-Bell

and Lynden-Bell [1] studied dwarf galaxies and determined rotational velocity of the Galaxy upto large distances.

For any test system moving under the influence of the gravitational field of the Galaxy, using the equation of motion and the virial theorem:

$$\frac{1}{2}\frac{d^2|r|^2}{dt^2} - v^2 = V_c^2 \tag{3.3}$$

where v is the velocity of that subsystem with respect to the Galaxy center and V_c is the circular velocity. Averaging the above equation over the subsystem and assuming virialisation one gets the Frenk-Lynden-Bell result.

$$\langle v^2 \rangle = \langle V_c^2 \rangle \tag{3.4}$$

Since DS galaxies are beyond 50 kpc, information on the velocities of these galaxies can be used to constrain the rotational velocity of the Galaxy at large distances. If the distribution is isotropic then it is very easy to see that

$$\langle v^2 \rangle = (\mu + 1)v_r^2$$

for which $\mu = 2$; where v_r is the radial velocity and v_t the transverse velocity and $\mu = v_t^2/v_r^2$. Even though the result in Eq [3.4] is for ensemble averages, Lynden-Bell and Lynden-Bell, considering the small number of DS available, assume that radial velocities of individual DS give a measure of the ensemble average and plot $V_c^2 = (\mu + 1)v_r^2$ for various galacto-centric distances, assuming $\mu = 2$ (Fig [3.4]). However, it is more likely that the distribution of dwarf spheroidals is anisotropic and indeed we do observe that there are no satellite galaxies below 50 kpc and above a certain galactocentric distance of 250 kpc. In this chapter we attempt to obtain the value of μ which can give a measure of the deviation from cisotropy, given the position and velocities of 8 satellite galaxies of the Local Group.

3.2 Rotation Curve at Large Distances

In the previous section we saw how the rms space velocity, $\langle v^2 \rangle^{1/2}$ related to the the rotational velocity. It can be argued that originally there were many DS probably with a wide spectrum of velocities and what survives today is only a skewed distribution of velocities. Using a simple potential model and energy considerations we attempt to find the allowed and possible existing velocities. This means that of all possible velocities there are only a few allowed velocities in the phase space.

Assumptions

(i) There is a minimum Galactocentric distance (r_{min}) for the DS which is about 78 kpc, below which there are no DS. There is also a maximum distance (r_{max}) which we have taken to be that of the galaxy LeoI at 245 kpc which is also the effective size of the halo (see Table[3.1]). We have varied these distances r_{max} and r_{min} to compute the values of μ.

(ii) We have assumed a Plummer distribution to model the visible matter of the Galaxy since at distances r > 20 kpc such an approximation of spherical potential is adequate. For larger distances, where the dark matter is a dominant component, we have chosen a logarithmic potential which is a general assumption to reproduce a flat rotation curve.

(iii) We assume that the line-of-sight velocity corrected to the galactic center of rest is the same as the radial velocity since at the large halo distances this difference between the direction of the Sun and the direction of Galactic center can be neglected.

(iv) We estimate the value of μ assuming simplified form for the potentials describing both the visible and dark matter.

$$\begin{aligned} \Phi_{vis} &= \frac{GM}{\sqrt{r^2+b^2}}; & b = 0.7\text{kpc} \\ \Phi_{DM} &= \frac{v_0^2}{2}\ln(R_c^2+r^2); & R_c = 7\text{kpc}, \quad v_0 = 220\text{km s}^{-1} \\ \Phi &= \Phi_{vis}+\Phi_{DM} \end{aligned} \tag{3.5}$$

Even at the outset we note that the estimates of μ are not very sensitive to these assumptions. The energy of a DS's motion can be written as

$$E = \frac{v_r^2}{2} + \Phi_{eff}(r) \tag{3.6}$$

$$\Phi_{eff} = \frac{L^2}{2r^2} + \Phi(r) \tag{3.7}$$

where L is the angular momentum of the system defined as $L = r_{in}v_t$, where r_{in} is the initial distance and v_t is the initial transverse velocity. Rewriting Eq [3.7] we see that

$$\frac{v_r^2}{2} = E - \Phi_{eff}(r); \tag{3.8}$$

In Fig [3.1] we plot the Φ_{eff} as a function of the of the distance. This graph is plotted for a typical value of L, *i.e.*, for a typical value of r_{in} and v_t. Two energy scales E_{in}, E_{max} can be identified with three length scales r_{in}, r_{min} and r_{max}. The energy scale E_{in} is fixed by the

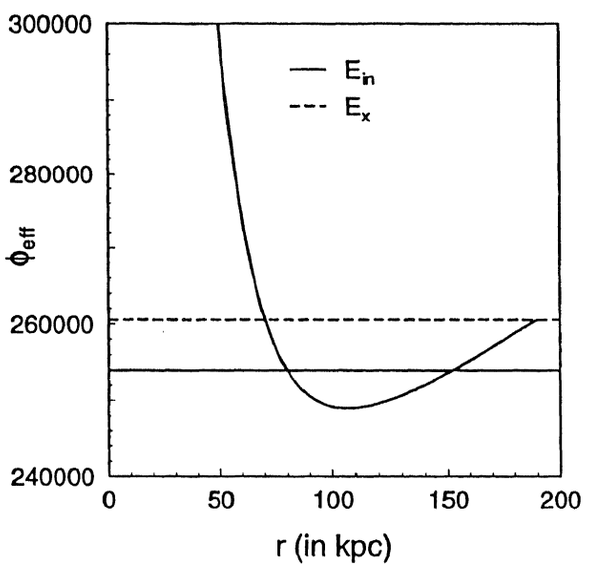

Figure 3.1: The figure is a typical plot of Φ_{eff} vs r and indicates the $E_{\rm in}$ and $E_{\rm x}$ whose difference sets the constraints on the allowed values of v_r *i.e.*, $\frac{1}{2}v_r^2 = E_{\rm in} - E_{\rm x}$.

initial position and the $E_{\rm max}$ is determined by either $r_{\rm min}$ or $r_{\rm max}$. For a particular choice of $r_{\rm min}$, the corresponding energy can be read off in the plot as $E_{\rm min}$ and for $r_{\rm max}$ there is a corresponding energy $E_{\rm x}$. For each choice of the angular momentum, the $E_{\rm max}$ is determined depending on which of the two energies is lower $E_{\rm min}$ or $E_{\rm x}$. In the Fig [3.1] we have the $E_{\rm max}$ is determined by $r_{\rm max}$ =190 kpc, (since this is lower than $E_{\rm min}$ corresponding to $r_{\rm min} \approx 50$ kpc) and the initial value of around 70 kpc. Essentially, the allowed orbits outside $r_{\rm min}$ and $r_{\rm max}$ are excluded.

3.3 Results and Discussion

We compute the allowed values of the radial velocities for all possible transverse velocities for initial values of the position ($r_{\rm in}$). Thus, the possible values of v_r are restricted, and in the Fig [3.2], we point out the region of these (v_t, v_r) values. We calculate the $\langle v_r^2 \rangle$ and $\langle v_t^2 \rangle$ values of the radial and transverse velocity component, averaging over the distribution function at each r. However, now the averaging is not over all the velocities but the restricted region, (v_t, v_r) that we have obtained. We have here, assumed an isothermal distribution function (Eq [3.11]) to model the DS.

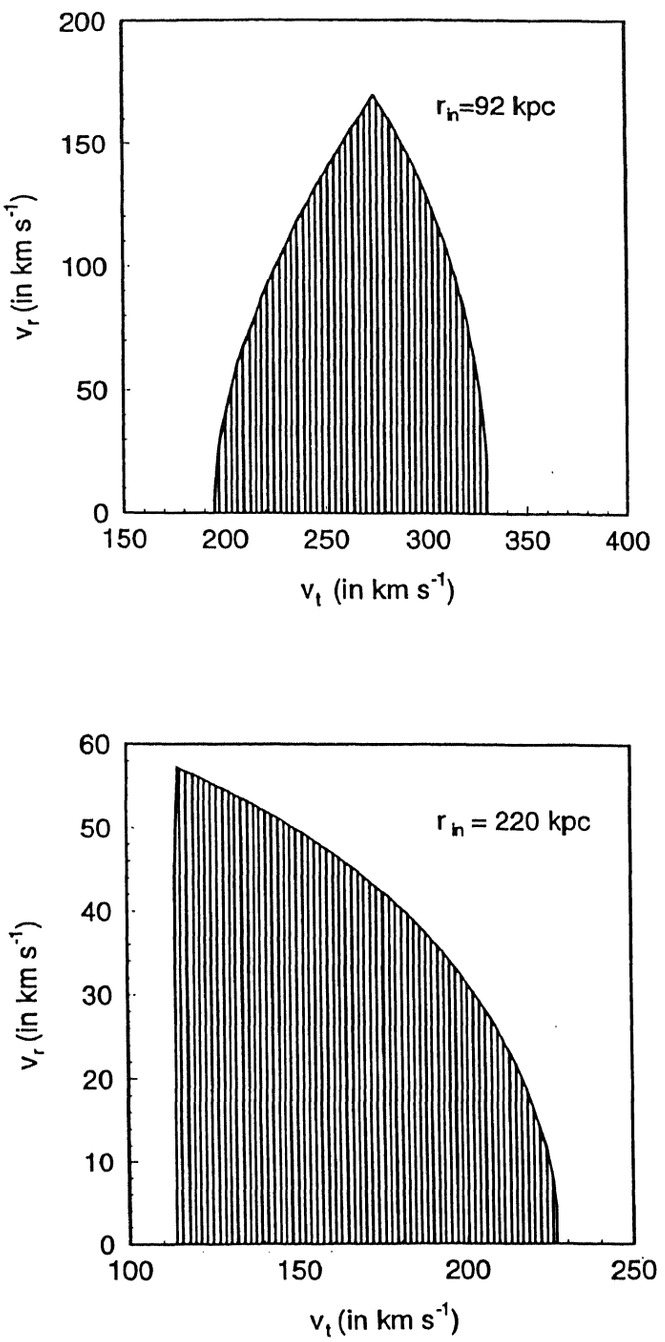

Figure 3.2: The allowed area in the (v_t, v_r) space for a given initial r_{in} is the shaded region

name	l	b	v_l in km/s	r(in kpc)
Carina	260.14	-22.20	14	119.7
Draco	86.37	34.71	-94	85.9
Sculptor	287.61	-83.16	74	86.0
sextans	243.50	42.27	78	101.5
UrsaMinor	104.98	44.81	-87	78.9
Fornax	237.16	-65.67	-34	150.7
Leo I	225.99	49.11	177	234.1
Leo II	220.14	67.23	16	245.9

Table 3.1: The line-of-sight velocities and distances of the DS

In general, the v_r^2 is calculated as given in the equation below. However now, the limits range from $v_{\rm rmin}$ to $v_{\rm rmax}$ for v_r and $v_{\rm tmin}$ to $v_{\rm tmax}$ for v_t.

$$\langle v_r^2 \rangle = \int\int f(r,v) v_t v_r^2 dv_r dv_t \tag{3.9}$$

$$\langle v_t^2 \rangle = \int\int f(r,v) v_t^3 dv_r dv_t \tag{3.10}$$

$$f(r,v) = \exp -(v^2 + \Phi(r))/\sigma^2 \tag{3.11}$$

where $\sigma = 220$ kms^{-1}.

For every initial value of $r_{\rm in}$ the $\langle v_{\rm r}^2 \rangle$ and $\langle v_{\rm t}^2 \rangle$ are calculated by averaging over the range of allowed velocities that we have computed earlier. If the distribution of DS were isotropic then the ratio of μ, which is obtained after doing a spatial averaging, is $\langle v_{\rm t}^2 \rangle / \langle v_{\rm r}^2 \rangle = 2$.

We compute the ratio $\mu(r)$ as a function of r from Eq [3.10–3.10]. In Fig [3.3] we show μ as a function of the galactocentric distance for an $r_{\rm min} = 78$, $r_{\rm max} = 245$ and $r_{\rm min} = 78$ and $r_{\rm max} = 200$. At the point $(r_{\rm min}, r_{\rm max})$ the value of μ rises sharply as expected since at these points the velocity motion in the radial component is minimal. The value of μ is sensitive to the choice of $r_{\rm min}$, $r_{\rm max}$ as is evidenced from the Fig [3.3].

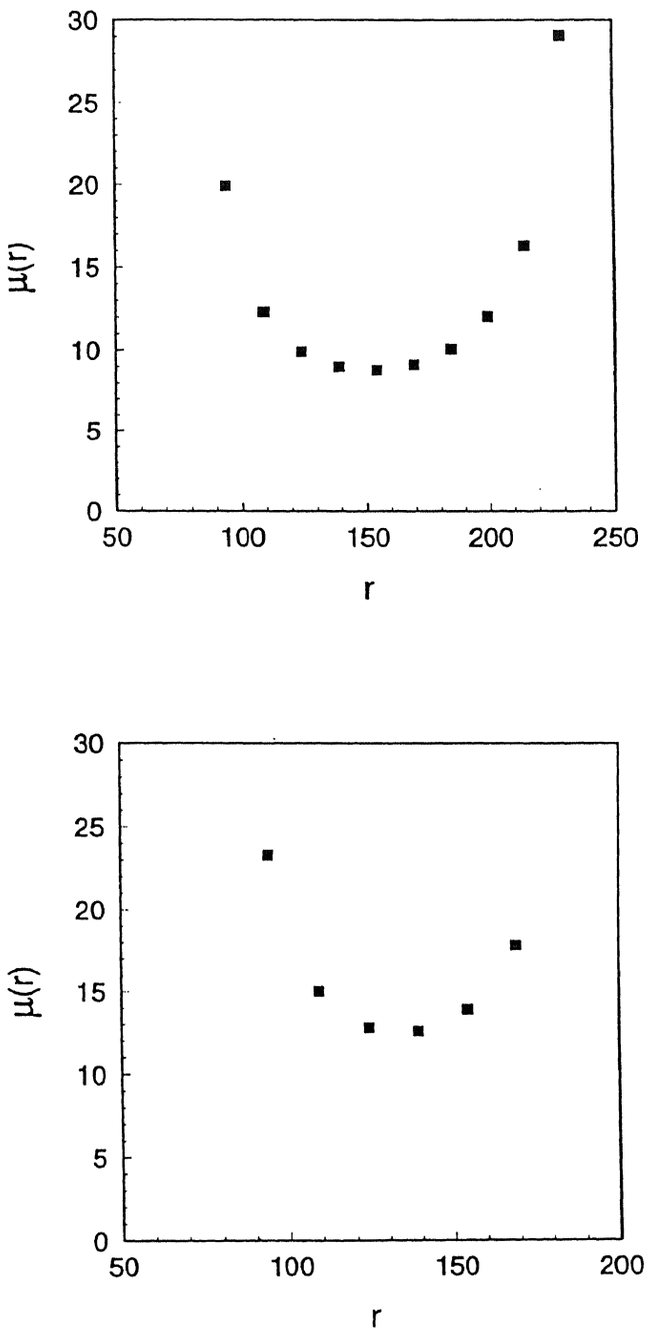

Figure 3.3: The graph shows the variation of μ vs r for r_{min} = 78 and r_{max} =245 & 200 in the first and second figure respectively

We saw earlier from Eq [3.4] that the

$$\langle v^2 \rangle = \langle V_c^2 \rangle$$

where

$$\langle v^2 \rangle = 3\langle v_l^2 \rangle$$

or this can be rewritten as

$$v^2 = v_r^2 + v_t^2 = v_r^2(1 + \mu)$$

where μ was 2. In this analysis the value of μ averages [1](see the top figure in Fig [3.3]) to 11.67, for a specific choice of $r_{\rm min}$ and $r_{\rm max}$ The value of the rotational velocity can be calculated using the equation below for a value of $\langle \mu \rangle = 11.67$

$$\langle V_c^2 \rangle = \langle v_r^2 \rangle (1 + \mu) \tag{3.12}$$

The Table [3.1] (from Ref [1]) below shows the values of the line of sight velocities and the radial distances. Since we have earlier assumed that the radial velocities can be approximated to the line of sight velocity, we compute the average value of $\langle v_r^2 \rangle^{1/2}$ which is 87 kms^{-1}. Using Eq [3.12] we obtain the average value of $V_c = 309$ kms^{-1}. The value of μ we have obtained is not very sensitive to the various parameters like σ and v_0. It is nevertheless, sensitive to the choice of $r_{\rm min}$, $r_{\rm max}$ and $r_{\rm max} - r_{\rm min}$. In Table [3.2] we show the value of μ for various values of $r_{\rm min}$ and $r_{\rm max}$. The value of V_c have seen depends crucially on the spatial distribution of the dwarf spheroidals and any change in these values could result in very different rotational speeds as can be seen from Table [3.2] However when we compute this ratio using the above analysis then it is clear that this value is much larger and of the order of 5 or more. This is expected because at the boundaries, the motion of the particles is entirely transverse rather than radial we have also taken into account the skewed spatial distribution of these galaxies. We can also argue that one would expect more transverse than radial motion else the system would have been tidally disrupted. The above analysis gives a measure of the deviation from isotropy which can be used to calculate the rotation velocity directly.

Since there is a maximum distance beyond which the DS are not found it is probably more appropriate to model the DS distribution by a King's DF. In the King's model velocity goes to zero at the tidal radius (beyond which there are no DS) $r_t = r_{\rm max} = 245$ kpc. However, in this case there has to be another cutoff because there are no DS at short distances also. Therefore the velocity will again vanish at $r_{\rm min} = 78$ kpc. By measuring the radial velocities

[1]Note that this value is obtained by a spatial averaging of $\mu(r)$

μ	r_{min}	r_{max}	V_c in kms^{-1}
11.67	78	245	297
16.16	78	200	360
33.23	78	150	509
12.31	50	150	317.4
6.6	50	245	239
8.318	50	200	265
58.297	150	245	673.7
176.505	150	200	1157

Table 3.2: We show that the value of rotation curve V_c changes drastically by changing the distance between the DS.

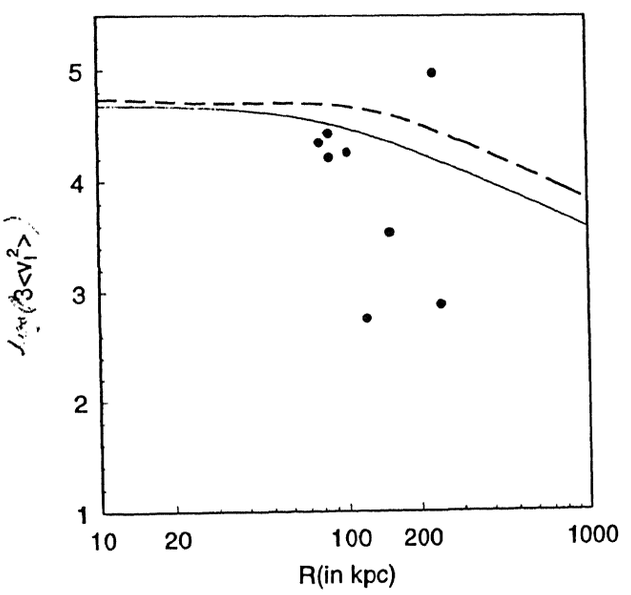

Figure 3.4: The value of $\log(3v_l^2)$ vs log(R) is compared with the a theoretically obtained rotation curve V_c using the King's model with a tidal cutoff radius of 300 kpc which is shown by the line. The rotation curve due to a spheroidal distribution is also plotted with dashed line.

of a set of objects like dwarf spheroidals we want to derive the V_c at large distances. However, Eq [3.4] is valid only when the averaging is done over the entire ensemble rather than on a subset of particles contained in a radial interval. Therefore the $V_c(r)$ we obtain in this fashion is only a *lower bound.* Lynden-Bell and Lynden-Bell [1] assumed a spheroidal distribution and modelled the DS.

In Fig [3.4] we show the theoretically calculated V_c for a tidal radius of 300 kpc and the $3\langle v_l^2 \rangle$ for the dwarf spheroidals and this should be taken as a lower bound. This calculation has been done assuming a value of $\mu = 2$

We have obtained a value of V_c which is larger than what one would obtain by extrapolating the rotation curve under the assumption of flatness at large distances. We have demonstrated that at large distances, the rotational velocity is probably not the same value that of 220 kms^{-1}at 20 kpc. As we saw in the earlier chapter that the velocity dispersion of 600 $kms^{-1}$is consistent with the rotation speed at the Solar neighborhood and this value can be used to constrain the rotation curve at large distances. The value of 309 $kms^{-1}$and the other values of rotation speed depending on the exact distances of the DS we have derived here seems to be consistent with this earlier calculation. It is clear that better observations will enable better determination of rotation speeds at large distances.

Bibliography

[1] Lynden-Bell, D., & Lynden-Bell, R.M., 1995, MNRAS, 275, 429

[2] Aaronson, M., 1983, ApJL, 266, L11

[3] Pryor, C., 1992, ASS, 163, *Morphological and Physical Classification of Galaxies*

[4] Lake, G., 1990, MNRAS, 244, 705

[5] Eggen, O.J., Lynden-Bell, D., Sandage, A.R., 1962, ApJ, 136, 748

[6] Moore, B. astro-ph/9511147

[7] Toomre, A., & Toomre, J., 1972, ApJ, 178, 623

[8] Lynden-Bell, D., Cannon, R.D., & Godwin, P.J., 1983, MNRAS, 204, 87p

[9] Little, B., & Tremaine, S., 1987, ApJ, 320, 493

[10] Kulessa, A.S., Lynden-Bell, D., 1992, MNRAS, 255, 105

[11] Cowsik, R., & Ghosh, P., 1986, JAA, 7, 7

[12] Lynden-Bell, D., & Frenk, C.S., 1981, Observatory, 101, 200

Chapter 4

Event Rates and Velocity Dispersions

This chapter focuses on an entirely different aspect of the dark matter problem, that of detecting a dark matter candidate. In this chapter we have two main sections: Section [4.1] presents some of the experiments to detect non-baryonic dark matter. Section [4.2] puts our work in perspective and presents the theoretical framework required to understand the data that is presently the available to us. We obtain new bounds and constraints on the scattering cross section of dm-particles as a consequence of the large $\langle v^2 \rangle_{\rm DM}^{1/2} = 600$ kms^{-1}we have obtained in the earlier chapter. We have already briefly discussed the several possible candidates in the Chapter 1, namely, neutrinos, WIMPs and the axions. We learn that since their interaction cross section is small, the detection of these particles poses a major problem.

4.1 Detection of Dark Matter

It is clear that the number of possible particles is very large given the several possible extensions of the standard model of particle physics. In literature, there are several articles which describe the particles and their detection at great length [1, 2]. The general difficulty of detecting any hypothetical dark matter particle stems from the fact that they are neutral, weakly interacting and have very low energy. Particle detection is based on transfer of energy by the dark matter particles to electrons in a detecting apparatus. Charged particles and photons can be detected easily whereas neutral particles are usually detected by utilizing an interaction or a sequence of interactions to produce charged particles. For example, neutrinos can be detected by conversion to electrons in a scattering process or by a transfer of kinetic energy to a nucleus which can then result in further ionisation and this kind of detection is

termed as "direct detection". The indirect detection involves detecting primary interaction that take place outside the earth for e.g in the sun, to produce a secondary flux of particles.

In this chapter we focus on direct detection techniques. The direct detection techniques fall into two classes: (i) those for heavy particles, with interactions comparable to the standard weak interactions and (ii) those for light bosons, with much lower coupling. Heavy weakly interacting particles become detectable because the interaction cross-section is proportional to the square of the mass, M_{D}^2. The maximum energy transferred on collision with the nucleus also increases with M_{D} and this energy is in the range of eV, for masses greater than 1GeV. These nuclear recoils are in principle observable either through the production of phonons (detected through a small change in temperature or directly as pulses of ballistic phonons) or through a small fraction of energy that is converted to ionisation energy.

In the case of the light boson (axion), the interaction coupling to matter is much weaker than that WIMPs and hence produces a smaller number of individual scattering events. It was later pointed out by Sikivie [3] that larger event rates would result from coherent conversion of axions to photons in vacuum. Axions couple to two photons via vacuum loops of charged leptons and quarks. A source of photons will convert an axion into a photon with energy equal to the axion mass so that all the photons produced will lie in a narrow frequency band, essentially in the microwave/infrared range for cosmologically significant axions. Significant event rates would result with practical volumes and magnetic fields.

The primary problem with the detectors of dark matter is the high background noise and therefore effort is directed towards designing ultralow background detectors. It is also important that the detectors have a low threshold energy so as to enable better detection of the low energy dark matter signal [4, 5]. The three main signatures of a dark matter signal are the recoil spectrum, annual and diurnal modulation of the recoil spectrum. The modulation signals has been thought to be very definitive signature of a detection; however so far the very many attempts at detection of DM particles have not yielded conclusive results. Comparison of predicted dark matter event rates with the experimentally measured rate has been so far useful to exclude or constrain regions in the mass cross-section parameter space. Besides the experimental difficulties of high back ground noise, there are theoretical uncertainties ranging from Galactic models to the inputs from particle physics

(i) Hot and Cold Dark Matter

One of the first non-baryonic particles that has been a "hot" favorite for many years has been the neutrino. With the results of the Superkamiokande experiment [6] the existence of a neutrino with non-zero mass has been confirmed. Neutrinos are referred to as "hot" because they have relativistic velocities at the time of decoupling from thermal equilibrium in the early universe. The reason they went "out of fashion" was because within the existing structure formation theories and the results of COBE the HDM model, they had too little power on smaller scales.

The WIMPs are particles of cold dark matter (*i.e.*, non-relativistic at the time of decoupling). There are many particles that belong to this category and the mass range is $M_{\rm WIMP} \gtrsim 3\,{\rm GeV}$. Since these exotic particles are in the regime of physics beyond the standard model there has been a surge of experiments designed to detect these WIMPs. Currently one the most sensitive experiments are the Heidelberg-Moscow experiments about which we shall discuss in detail because the data for the studies in this chapter is obtained from these experiments.

4.1.1 Experiments and Detectors

(i) The AMANDA Collaboration

The AMANDA experiment is designed for the indirect detection of dark matter particles. The basic idea is that the WIMPs in the halo occasionally scatter in the interior of the Earth and Sun and lose enough energy to be gravitationally trapped. They then gradually fall in the center where they accumulate. Since neutralinos (a WIMP candidate) are their own antiparticles, they will annihilate when they encounter each other. Then annihilation products will generate neutrinos of energy comparable with the mass of the neutralino, in the range of 10-100 GeV and they can be detected by AMANDA. The AMANDA setup has been designed to track the upward going neutrino candidates to avoid those due to cosmic ray muons which penetrate the over-burden of ice. The successful deployment of a 4-string AMANDA-A array with photomultipliers (PMTs) was the first step towards demonstrating that the South Pole ice is a suitable site for high-energy neutrino observatory. With a hot-water drill, four holes 60cm in diameter were created during the 1993-94 season and instrumented with 80 PMTs spaced at 10-m intervals. One of the most favorable signals to search for, using this apparatus, would be the high energy neutrinos from the center of the

Earth. If no signal is found, useful limits can be derived on the parameters of SUSY model [7]

(ii) Superheated droplet detectors(SDD) as CDM detectors

The SDD's are useful and advantageous for WIMP detection. These devices consist of a dispersion of droplets of a superheated liquid fixed in a viscous polymer or aqueous gel. The greatest advantage of SDD's are that they are sensitive only to high linear energy transfer (LET) radiation and therefore energetic muons, gamma rays, x-rays and beta particles fall well below the activation threshold (typically $> 200\text{keV}/\mu m$). The SDD is optimal for the exploration of the spin dependent neutralino coupling. This idea is in the form of the experiment SIMPLE (Superheated Instrument For Massive Particle Experiments) [8]

(iii) WIMP-nucleon cross section from the cryogenic dark matter search

As mentioned earlier the WIMPs have been a challenge to detect and many detectors are being designed to detect them. Among them, the cryogenic those which are Ge or Si semiconductor detectors in a shielded background cryostat. The CDMS experiment in particular is useful in distinguishing the electron-recoils which are primarily due to background photons and the nuclear recoils which are because of the WIMPs. This is possible because the nuclear recoils are less ionizing [9].

(iv) Double beta decay experiments

Nuclear double beta decay has a good potential to probe the physics beyond the standard model. The current best sensitivity especially in the sub-eV region is obtained to a large extent by the Heidelberg-Moscow double beta decay experiments.

In this thesis we use the data obtained from these experiments. Double beta decay can occur in several decay modes

$$
\begin{aligned}
{}^{A}_{Z}X &\rightarrow {}^{A}_{Z+2}X + 2e^{-} + 2\overline{\nu}_{e} \\
{}^{A}_{Z}X &\rightarrow {}^{A}_{Z+2}X + 2e^{-} \\
{}^{A}_{Z}X &\rightarrow {}^{A}_{Z+2}X + 2e^{-} + \phi \\
{}^{A}_{Z}X &\rightarrow {}^{A}_{Z+2}X + 2e^{-} + 2\phi
\end{aligned}
$$

The experiment was initially set up to search for neutrinoless beta-decay. Later additional

enriched detectors were used to search for the WIMPs. While the earth is moving through the dark halo, some WIMPs will scatter with the nuclei in the detector giving a small but detectable ionisation. A major part of the energy goes into thermal excitations and only a small fraction gets converted into ionisation. For the Ge in the detector, the relative ionisation is about 25-30% and therefore a sufficiently low detector threshold of $\leq$ 10 keV is required. This experiment has been used to set limits for the first time on coherent-cross section of spin-independently interacting WIMPs.

The experiment searches for the last three modes of decay which are neutrinoless decay modes. The largest sensitivity for the $0\nu\beta\beta$ is obtained at present by such active detector experiments. Depending on the nature of the particles and the detector material used, the scattering is either spin dependent or spin independent. The typical recoil energy of the nucleus in the detector reaches up to 10-100 keV, depending on the mass of the WIMP. Currently the sensitivity obtained by the Heidelberg-Moscow experiment is of the order of 0.1-0.2 eV [10, 11, 12, 13]. With five enriched detectors (86% of ^{76}Ge) of a total mass of 11.5 kg taking data in the Gran Sasso underground laboratory and with a background that is 0.07 counts/kg year keV, the experiment has stabilised and is now exploring the energy deposition in the sub eV by the dark matter particles.

4.2 Motivation

While a general motivation has already been mentioned earlier we are reemphasising it because the context is appropriate to do so. The important parameters that go into the calculation of any event rate are the density, the velocity, and cross section of interaction of the dark matter particles with the detector. The determination of the dark matter density in the Solar neighborhood, $\rho(R_\odot)$ has been a controversial problem. There have been self consistent dynamical calculations that determine the density to be $0.3\,\mathrm{GeV cm^{-3}}$ [14]. Conflicting values for the $\rho(R_\odot)$ have been reported by Kuijken & Gilmore [15]. However the $\langle v^2\rangle_{\rm DM}^{1/2}$ for the dark matter particles has been *assumed* to be of the order of 270 $\mathrm{kms^{-1}}$. On the other hand our analysis in Chapter 2, on the basis of a two component model for the Galaxy indicates that the $\langle v^2\rangle_{\rm DM}^{1/2} = 600$ $\mathrm{kms^{-1}}$.

In the next section we review the theoretical framework in which event rates in detectors are calculated. This is followed with a discussion of the experimental data, the analysis used to compare predicted and experimental rates, and the conclusions reached.

4.2.1 Theoretical Framework

Weakly interacting particles (WIMPs), on interacting with the detector nucleus are expected to produce a certain event rate. We compute this event rate and compare it with the experimental rate, and thus obtain limits on the mass and cross-section of the WIMP particles. The interaction cross-section remains a free parameter whose value is determined by comparing the experimental and calculated event rates for any given mass of the WIMP particle. Particle detection is based on the transfer of energy from the WIMPs to the detector nuclei. This transfer of energy is in the form of either nuclear recoil energy or ionisation energy. The experiments measure the events per day per kilogram of the detector material as a function of the energy deposited [17].

The total event rate can be approximated as $R \approx n\sigma\langle v\rangle/m_{\mathrm{N}}$ where $n = \rho_0/m_\chi$, where ρ_0 is the central density and m_χ is the mass of the dark matter particle, σ is the elastic cross section, $\langle v\rangle$ is the average speed of the WIMP relative to the detector and m_{N} is the nuclear mass of the detector nuclei. To calculate a more realistic total event rate one should take into account (1) the WIMPs motion in a halo with a distribution of velocities $f(v)$ which also incorporates the earth's motion, (2) form factor, that arises mainly due to the finite size of the nucleus and depends principally on nuclear radius and recoil energy and (3) threshold energy E_T of the detectors.

The differential rate can be written as

$$dR = \left(\frac{\rho_0}{m_\chi m_{\mathrm{N}}}\right) v f_1(v)(d\sigma/d|\mathbf{q}|^2)d|\mathbf{q}|^2 \tag{4.1}$$

This differential form has all the ingredients of the earlier specified total rate except for the inclusion of the distribution of speeds relative to the detector, $f_1(v)$ found by integrating $f(v)$ (the three dimensional velocity distribution) over all angles. The total rate is obtained be integrating the differential rate from E_t to infinity. The momentum transferred is given by

$$|\mathbf{q}|^2 = 2m_r^2 v^2(1 - \cos\theta)$$

where θ is the scattering angle in the center of momentum frame, and m_r, the reduced mass by $m_r = m_\chi m_{\mathrm{N}}/(m_\chi + m_N)$; the energy deposited in the detector can then be written as

$$E_{\mathrm{R}} = |\mathbf{q}|^2/(2m_{\mathrm{N}}) = (m_r^2 v^2/m_{\mathrm{N}})(1 - \cos\theta) \tag{4.2}$$

The differential rate can now be rewritten as

$$\frac{dR}{dE_{\mathrm{R}}} = \frac{\sigma_0\rho_0}{2m_\chi m_r^2} F^2(E_{\mathrm{R}}) \int_{v_{\mathrm{min}}}^{\infty} \frac{f_1(v)}{v} dv \tag{4.3}$$

where

$$v_{\rm min} = \frac{E_{\rm R} m_{\rm N}}{2m_r^2}$$

where $F(E_{\rm R})$ is the form factor which should be chosen appropriately for scalar WIMPs and for WIMPs with the spin-dependent coupling. As a first approximation, the form factor can be understood as the Fourier transform of the density distribution of the scattering centers. In the calculation here we have chosen $F^2(E_{\rm R}) = \exp(-E_{\rm R}/E_0)$ where E_0 is the coherence energy, $E_0 = 3\hbar/2MR^2$ with M and R being the mass and root mean-square radius of the nucleus. This implies $E_0 = 49.1\,\mathrm{keV}$, for Ge. This form factor is that of a solid sphere approximating spin-independent interaction with the whole nucleus; σ_0 and ρ_0 are the cross section and the Solar neighborhood density of the dark matter particles respectively. The above equation (Eq [4.3) has been written such that all the dependence on the WIMP velocity has been put into one integral.

$$\frac{dR}{dE_{\rm R}} = \frac{\sigma_0 \rho_0}{\sqrt{\pi} v_0 m_\chi m_r^2} F^2(E_{\rm R}) T(E_{\rm R}) \tag{4.4}$$

where

$$T(E_{\rm R}) = \frac{\sqrt{\pi}}{2} v_0 \int_{v_{\rm min}}^{\infty} \frac{f_1}{v}(v)dv \tag{4.5}$$

In a isothermal model $v_0 = \frac{2}{3}\langle v^2 \rangle_{\rm DM}^{1/2}$. This is the way the velocity dispersion of the dark matter particles enters the calculation of the event rate. In the context of our model this is 600 kms^{-1}.

In the earlier chapter we discussed in detail the choice of the distribution function (DF); now we use the same DF in the calculation of rates here. Taking in to account the motion of the earth in the halo the distribution of speeds $f_1(v)$ of the dark matter particles is given by

$$f_1(v)dv = \frac{vdv}{v_e v_0 \sqrt{\pi}} \left\{ \exp\left(-\frac{(v - v_e)^2}{v_0^2} \right) - \exp\left(-\frac{(v + v_e)^2}{v_0^2} \right) \right\} \tag{4.6}$$

where v_e is the velocity of the earth chosen to be 245 kms^{-1}. Thus

$$\frac{dR}{dE_{\rm R}} = \frac{\sigma_0 \rho_0}{4 v_e m_\chi m_r^2} F^2(E_{\rm R}) \left[\mathrm{erf}\left(\frac{v_{\rm min} + v_e}{v_0} \right) - \mathrm{erf}\left(\frac{v_{\rm min} - v_e}{v_0} \right) \right] \tag{4.7}$$

(i) Dark matter density and the velocity dispersion of the WIMPs

The local density, $\rho(R_\odot)$ and $\langle v^2\rangle_{DM}^{1/2}$ are the two free parameters of a Maxwellian distribution function and it is important to determine them correctly and consistently. We have already discussed this determination of $\rho(R_\odot)$ and $\langle v^2\rangle_{DM}^{1/2}$ in earlier chapters. We use a value of $\rho(R_\odot) = 0.3\,\mathrm{GeVcm^{-3}}$ which translates to the same value of surface density as used by Bahcall *et al.* . We illustrate our calculation with two choices of $\langle v^2\rangle_{DM}^{1/2}$: 270 $\mathrm{kms^{-1}}$and 600 $\mathrm{kms^{-1}}$.

4.3 Results and Discussion

We have used the Heidelberg-Moscow $\beta\beta$ experiment data for our analysis here. In their analysis, an $\langle v^2\rangle_{DM}^{1/2}$ assumed to be 220 $\mathrm{kms^{-1}}$, has been used to obtain the excluded region in the cross section mass parameter space. On changing this to 600 $\mathrm{kms^{-1}}$we get different bounds in this parameter space. We use differential rate data obtained from the above experiment to compare with the theoretically obtained event rate [4.7] for any given mass of the WIMP particle. We show the recoil spectrum below Fig [4.1] for both the values of the velocity dispersion $\langle v^2\rangle_{DM}^{1/2} = 270$ $\mathrm{kms^{-1}}$and $\langle v^2\rangle_{DM}^{1/2} = 600$ $\mathrm{kms^{-1}}$and for $m_D = 26$ GeV and 1 TeV. In Fig [4.1] we show the upper bound on the interaction cross-section σ for 2 values of $\langle v^2\rangle_{DM}^{1/2}$.

We have used the gradient method to do the least square fit for each mass of the WIMP particle, keeping the cross section as a free parameter in the problem. This method gives the exclusion plot for the masses and cross-section of WIMP particles. The exclusion plot for the two different velocity dispersions is shown in the figure below. It is interesting to note that for a larger value of the dispersion, a lower mass of the WIMP does not fit the lower energy spectrum very well.

(i) Distinct signals of dark matter component

The main problem with the recoil spectrum is that it is very difficult to obtain a clear signal of the dark matter component because of the high back ground noise. Thus what one has detected so far is, in some sense, the background noise which in turn allows certain regions of parameter space to be excluded. This is basically the exclusion plot that we have derived in Fig [4.2].

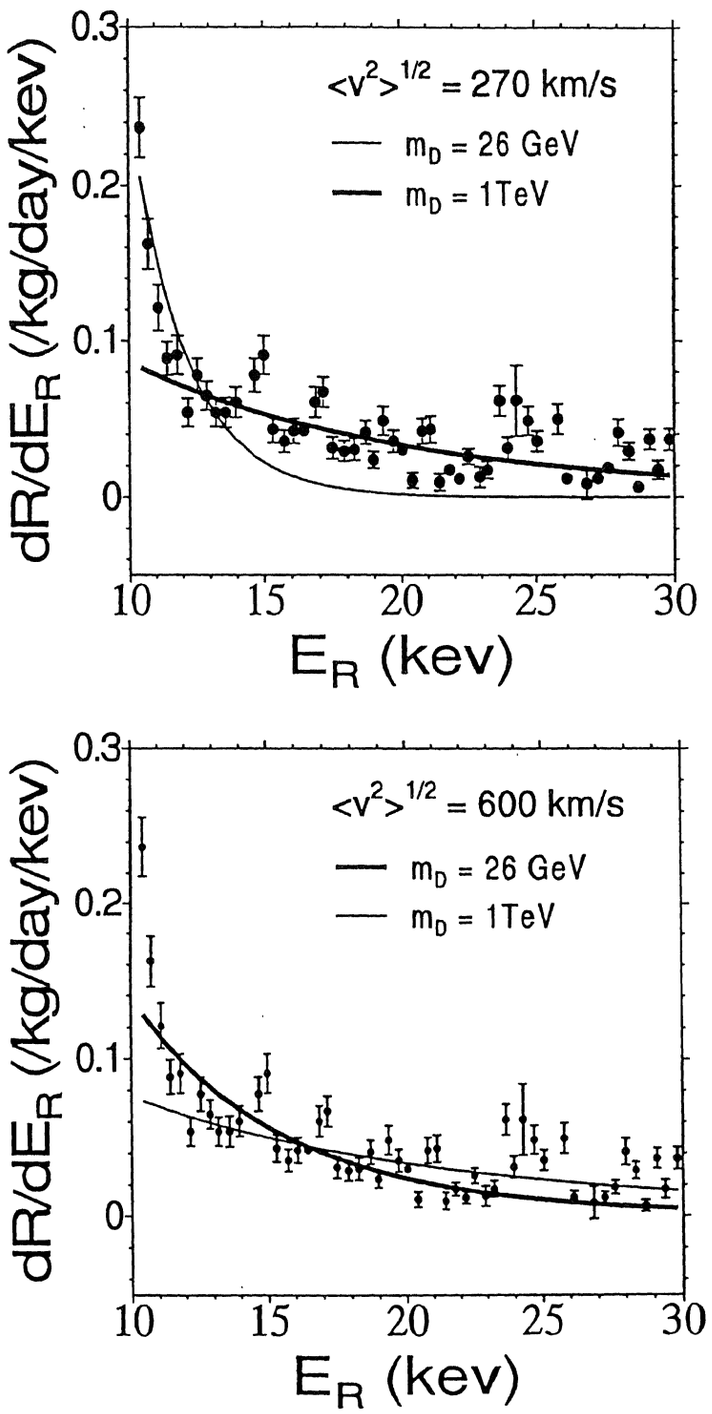

Figure 4.1: The predicted recoil spectrum compared with the Heidelberg-Moscow data for the two masses indicated in the figures for two different $\langle v^2 \rangle_{DM}^{1/2} = 270$ kms^{-1}and $\langle v^2 \rangle_{DM}^{1/2} =$ 600 kms^{-1}

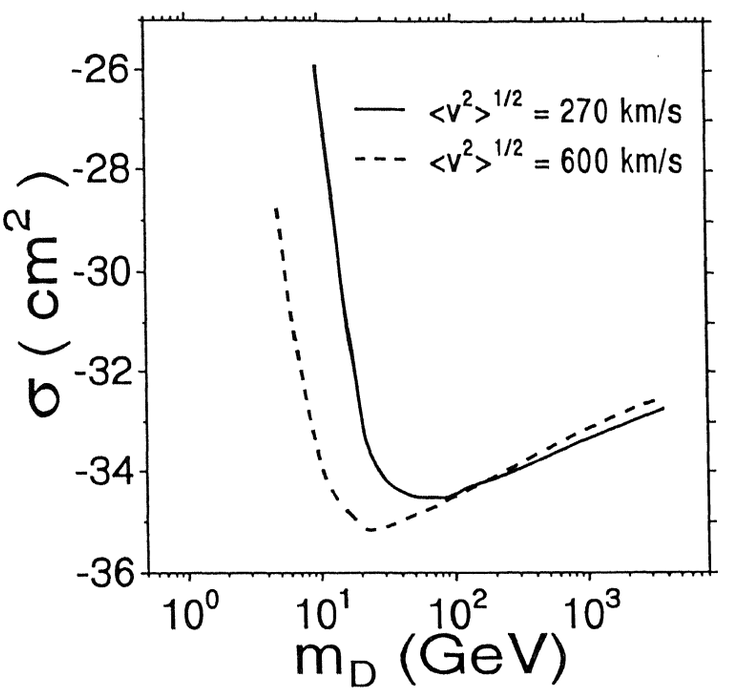

Figure 4.2: The exclusion plot in the mass cross-section parameter space is shown for two velocity dispersions. The line indicates the exclusion plot for an $\langle v^2 \rangle_{\rm DM}^{1/2} = 270$ kms^{-1}while the dotted line indicates the same for $\langle v^2 \rangle_{\rm DM}^{1/2} = 600$ kms^{-1}

(ii) Annual and Diurnal modulation

It is important that DM signatures somehow contrives to avoid the presence of the background. The annual and diurnal modulation of signals are two such possible indicators. The diurnal modulation relies on the effects of scattering of the dark matter particle with the Earth. The WIMPs scatter off elastically, giving rise to to variations in flux and speed distribution of the WIMPs arriving at the detector. Two times t_1 and t_2 are then chosen where the predicted scattering effects differ the most and the experimental data at these two times are then compared.

The Earth moves around the sun, with an orbital speed of 30 kms^{-1}in an orbit whose axis makes an angle of $\delta = 30°$ with respect to the velocity vector of the Sun. The sun also moves around the Galaxy at a velocity of 232 ± 20 kms^{-1}. The resulting net speed of the Earth its velocity with respect to the halo reference frame oscillates with a period of one year,

with maximum and minimum values in June and December respectively. Since the Earth's velocity enters in the calculation of the event rate (Eq [4.7]) it modifies the recoil spectrum. Thus, there should be seasonal changes of the recoil spectrum which should be measurable; *i.e.*, the recoil spectrum is modulated. The signal can be expressed as a constant term plus a modulation component:

$$S(t) = S_0 + S_m \cos[w(t - t_0)] \tag{4.8}$$

where S is the detection rate at any given time.

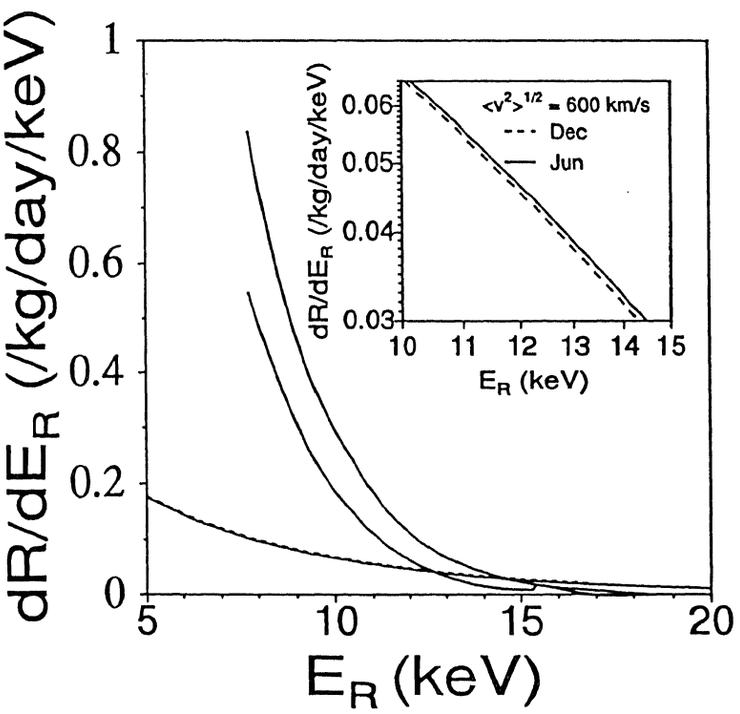

Figure 4.3: The recoil spectrum at two different time points for two different velocity dispersions is shown in the figure. To emphasis the fact for $\langle v^2 \rangle_{\rm DM}^{1/2} = 600$ kms^{-1}recoil spectrum are two distinct lines we have them in the inset as two distinct spectrum for June and Dec in the log scale.These spectra are obtained for a $m_D = 26$GeV.

In Fig [4.3] the recoil spectra for June and December are plotted for the two different velocity dispersions of 270 kms^{-1}and 600 kms^{-1}. It is very clear from the plots that for the larger $\langle v^2 \rangle_{\rm DM}^{1/2}$ the annual modulation signal is reduced quite drastically.

Here we re-derive the mass cross-section bounds for both these values of velocity dispersion.

By comparing the calculated rate with the observed values we find that the interaction cross-section is less than 4×10^{-35} cm^2 and 4×10^{-33} cm^2 for particle masses 26 GeV and 100 GeV respectively. We also find that the annual modulation signal is significantly reduced for a larger $\langle v^2\rangle_{DM}^{1/2}$ which immediately implies that one needs to go for better detectors to make any definite statement about the dark matter component.

Bibliography

[1] Smith, P., & Lewin, J.D., 1990, Phys. Rep. 187, 203

[2] Jungman, G., Kamionkowski, M., & Griest, K., 1996, Phys. Rep, 267

[3] Sikivie, P., Phys.Rev.Lett., 1953, 415; *ibid.*, Phys. Rev.D., 1985, 32, 2998

[4] Abriola, D., *et al.* , 1993, Astropart.Phys., 6, 63

[5] Beck. M., *et al.* , 1994, Phys.Lett.B, 336, 141

[6] The Super-Kamiokande collaboration, Learned, J.G., *et al.* , astro-ph/9705197, Fukuda, Y., *et al.* , hep-ex/9805006

[7] Bergstorm, L., *et al.* , astro-ph/9612122

[8] Collar, J.I., *et al.* , astro-ph/9610266

[9] Akerib, D.S., *et al.* , astro-ph/9712343

[10] Heidelberg-Moscow collab, Phys.Lett.B., 1995, 356, 450

[11] Heidelberg-Moscow collab, Phys.Rev.D., 1997, 55, 54

[12] Klapdor-Kleingrothaus, H.V., 1994, Progr.Part.Nucl.Phys, 32, 261

[13] Klapdor-Kleingrothaus, H.V., NEUTRINO 96, Helsinki, June 1996, World Scientific Singapore 1997, 317

[14] Bahcall, J.N., 1984, ApJ, 276, 169

[15] Kuijken, K., and Gilmore, G., 1989, MNRAS, 239, 571 ; *ibid.* 1989, 239, 605 ; *ibid.* 1989, 239, 651 ; ApJL, 1991, 367, L9

[16] Binney & Tremaine, 1987, *Galactic Dynamics*, Princeton University Press

[17] Lewin, J.D., & Smith, P.F., 1996, Astropart.Phys., 6, 87 and Phys.Lett.B, 1997, 407, 219

[18] Cowsik, R., Charu Ratnam., Bhatacharjee, P., 1996, Phys.Rev.Lett, 76, 3886

Chapter 5

Mass modelling and Halo Parameters of External Galaxies

So far we have used the model to study the distribution of dark matter in the Galaxy and its implications in the context of detector experiments. In this chapter we apply the model developed in Chapter 2 to other galaxies and study some properties of the dark matter halos in these galaxies. We have analysed 12 Sc, Sb galaxies with well defined rotation curves and luminosity profiles and study the halo parameters of each galaxy. From the luminosity profile we have determined the potential due to the visible matter in these galaxies. M/L values for the disk have been obtained by adopting a maximal disk solution as given by Kent [1]. Assuming the maximum amount of visible matter we derive the parameters of the DM-halo such as the central density and the velocity dispersion; consistent with the luminosity profile and the observed rotation curve.

In Section [5.1] we discuss the galaxies we have chosen and the observations of luminosity profiles and rotation curves. In Section [5.2] we discuss the modelling of galaxies and some of the results we have obtained.

5.1 Observations of galaxies

5.1.1 Luminosity Profiles and Rotation Curves

We have chose 12 Sc, Sb galaxies for applying the model we have developed in Chapter 2. We have chosen these galaxies because they have well defined HI rotation curves and luminosity profiles [1]. In the table below we list the galaxies we have chosen for our study. Assuming a specific M/L ratio it is straight forward to derive the visible matter distribution from the luminosity profiles.

Object	Type	D(Mpc)	components
N2403	Sc	0.67	disk
N2903	Sc	6.1	disk
N3198	Sc	9.2	disk
N4236	SBd	3.25	disk
N4258	Sb	6.6	disk
U2259	Sc	9.8	disk
N3031	Sb	3.25	disk+bulge
N2841	Sb	9.0	disk+bulge
N4736	RaSb	6.0	disk+bulge
N5033	Sbc	14.0	disk+bulge
N5055	Sbc	8.0	disk+bulge
N7331	Sb	14.0	disk+bulge

Table 5.1:

As is clear from the above table that we have 6 galaxies with both components: the bulge and disk component and the other 6 galaxies with only the disk component. The luminosity profiles for these galaxies are available in Ref [1]. All the photometric observations were done using the F and occasionally the J filters reduced to to r band of Thuan and Gunn [2]. The exposures were for typically 20 min on each and then the two dimensional frames were reduced and analyzed by Kent to yield major and minor axis luminosity profiles. The profiles are determined by fitting the isophotes with ellipses which are allowed to vary in position angle and ellipticity with radius. The main source of error was the sky background which is estimated to be 1%. For some of the galaxies the photometry is more uncertain.

The rotation curves for all the galaxies were obtained from various sources. All objects have HI observations and a few have optical rotation curves. The optical rotation curves are necessary to trace the potential of the inner part of the galaxy. Uncertainties in the inner regions of the galaxies could result in poor determination of the various parameters of the disk and bulge parameters.

5.2 Mass Modeling of the galaxies

The mass distribution of galaxies can be primarily decomposed into the visible and the dark matter component. The visible matter component comprises of the bulge and the disk. The luminosity profile gives a measure of these two components and therefore it can be used to deduce visible matter distribution. The rotation curve on the other hand gives a measure of the total potential of the galaxy which includes the dark matter component also.

Most disk components follow an exponential law and most bulges of galaxies are assumed to follow a DeVacouler's $r^{1/4}$ law. There have been various schemes outlined in the literature to decompose this luminosity profile into the disk and the bulge component [3, 4, 5]. The exponential disk can be written as $I(R) = I(0)\exp(-R/R_d)$; where $I(R)$ is in $L_\odot/pc^2$ and R is in kpc and the two constants $I(0)$, the central bulge luminosity and R_0 is the scale height.

We adopt a Hubble profile to describe the bulge profile given by

$$I_h(R) = \frac{I_0}{1 + (\frac{R}{a})^2} \tag{5.1}$$

where I_0 is the central density and a the core radius As mentioned earlier Kent's observations are done in the R band and since most observations of galaxies are done in the B band we have converted to the all the relevant observations to the B band to be consistent [6]. So essentially there are 4 parameters to be fit $I(0)$, R_d for the disk and $I(0)$, a for the bulge.

In obtaining a mass distribution we assume a constant M/L ratio independent of the radial distance. The M/L ratio is also decided by various methods and has been a matter of debate over the years. We start by assuming a maximum disk solution given by Kent *et al.* and fit the "visible " rotation curve in the inner part of the Galaxy where the forces are dominated by the visible matter. The potential obtained from the luminosity profile is used to fit only the "visible" rotation curve.

The results of fitting various galaxies with this procedure is given in terms of the values of the fitting parameters. Table I lists the values of the parameters in the order: (i) the central disk surface density (ii) total luminosity in the B-band,(iii) the exponential scale height(h) of the disk,(iv) the scale height in the bulge, (v) $(M/L)_{disk}$(vi) $(M/L)_{bulge}$ to the rotation curve. The surface density that we have obtained is consistent with that obtained by kent [1]. Some of the galaxies like N2259 and N4236 have rotation curves that do not extend very far and they have low rotational velocties. Not all the galaxies have an exponential fit but for our study here these details are not very important. The total luminosity in the disk is obtained by integrating the the the surface brightness to obtain $L = 2\pi h^2 I_0$ where h is the scale height

and I_0 is the value of the luminosity density at the center.

Name	Σ_0 $M_\odot pc^{-2}$	L($10^{10}L_\odot$)	h (in kpc)	a	$(M/L)_{disk}$	$(M/L)_{bulge}$
2403	185	0.516	1.903		1.87	
2903	200	1.29	1.81		3.35	
3198	150	8.57	2.48		2.05	
4236	80	0.265	2.675		2.34	
4258	200	2.62	5.28		3.08	
2259	80	0.64	1.34		5.0	
3031	240	1.46	1.98	0.287	1.76	2.76
2841	300	2.22	2.33	0.85	1.07	2.96
4736	180	1.07	1.85	0.14	0.84	0.599
5033	225	1.85	5.96	0.27	6.76	4
5055	220	2.51	3.73	0.068	4.03	4.3
7331	240	3.09	5.09	0.708	2.20	1.11

Table 5.2: parameters of the bulge and disk are listed in this table

The M/L values for the bulge and disk are obtained by fitting the inner part of the rotation curve. Having obtained the various parameters from the rotation curves and luminosity profile we go on compute the potential of the visible matter which will be an important input to our problem as seen in the Chapter 2. These parameters are important for obtaining the potential of the visible matter distribution

5.2.1 Potentials for the Disk and Bulge

As we noted earlier that the disk has an exponential light distribution and this kind of a distribution was first mass modelled by Toomre [7]. In Toomre's method the Laplace equation $\nabla^2\Phi = 0$ is solved subject to appropriate boundary conditions both at the disk and at infinity. In cylindrical coordinates the equation can be explicitly written as

$$\frac{1}{R}\frac{\partial}{\partial R}\left(R\frac{\partial \Phi}{\partial R}\right) + \frac{\partial^2 \Phi}{\partial z^2} = 0 \tag{5.2}$$

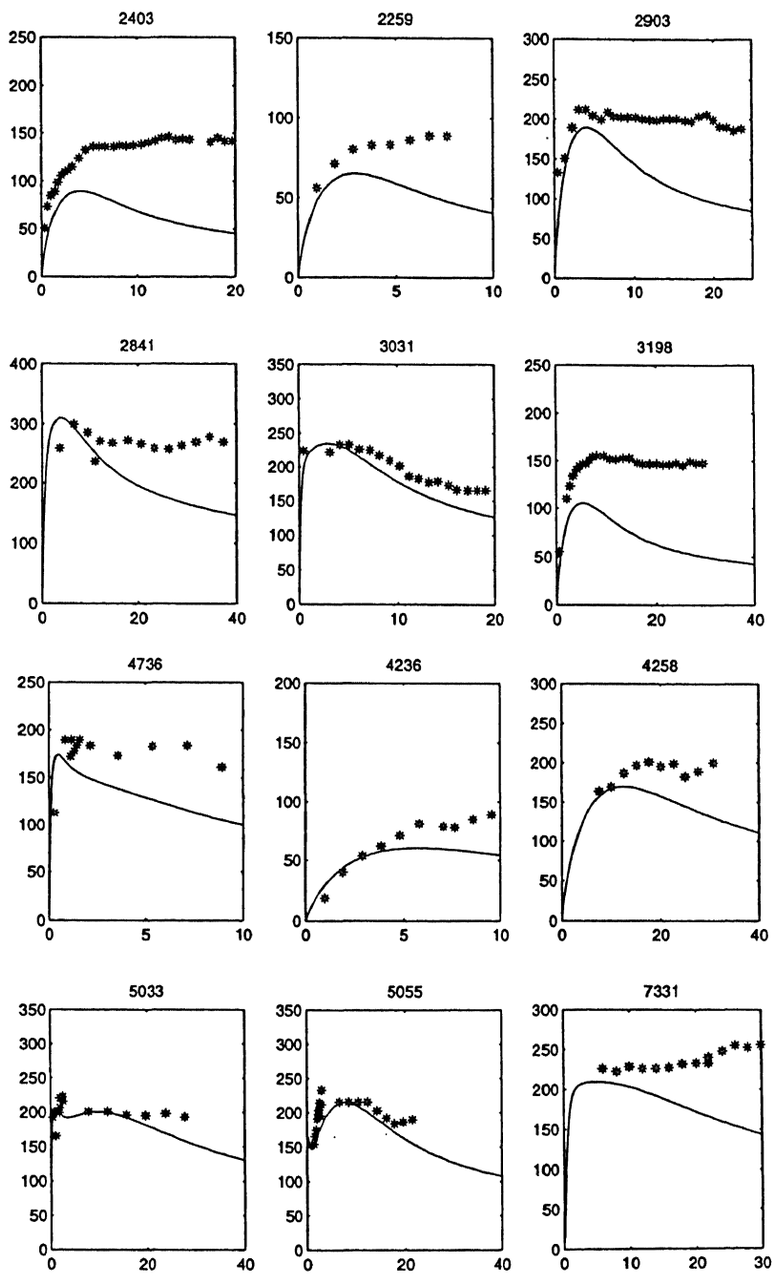

Figure 5.1: Rotation curves due to the disk and the bulge component

Using the method of separation of variables the solution for the above Laplace equation can be obtained as

$$\Phi_{\pm}(R,z) = exp(\pm kz)J_0(kR) \tag{5.3}$$

A generalised function of the form

$$\Phi_k(R,z) = exp(-k|z|)J_0(kR) \tag{5.4}$$

where k is real and positive and $\Phi_k(R,z)$ also solves the Laplace equation. Using Gauss theorem the surface density that generates the discontinuity can be calculated

$$\lim_{z\to 0^+}\left(\frac{\partial\Phi_k}{\partial z}\right) = -kJ_0(kR)$$

&

$$\lim_{z\to 0^-}\left(\frac{\partial\Phi_k}{\partial z}\right) = +kJ_0(kR)$$

from which it follows that surface density can be written as $\Sigma_k(R) = -(k/2\pi G)J_0(kR)$

This equation can be used to obtain the potential generated by an arbitrary surface density $\Sigma(R)$.

$$\Sigma(R) = \int_0^\infty S(k)\Sigma_k(R)dk = \frac{1}{2\pi G}\int_0^\infty S(k)J_0(kR)kdk \tag{5.5}$$

then we will have

$$\Phi(R,z) = \int_0^\infty S(k)\Phi_k(R,z)dk = \int_0^\infty S(k)J_0(kR)\exp^{-k|z|} \tag{5.6}$$

$$S(k) = 2\pi G\int_0^\infty J_0(kR)\Sigma(R)RdR \tag{5.7}$$

Eliminating $S(k)$ we obtain

$$\Phi(R,z) = -2\pi G\int_0^\infty dk\exp^{-|k|z}J_0(kR)\int_0^\infty \Sigma(R')J_0(kR')R'dR' \tag{5.8}$$

The surface density is obtained from the luminosity density, using value for the M/L as listed in Table [5.2] we obtain the potential as described by the above procedure. We use the modified Hubble profile which is a good description of most spherical density distribution like the bulges of galaxies and elliptical galaxies [8]. The potential is written as

$$\Phi_h = -\frac{GM_h}{R} - \frac{4\pi G\gamma j_0 a^2}{\sqrt{1+(r/a)^2}} \tag{5.9}$$

where

$$M_h = 4\pi a^3 \gamma I_0 \left\{ \ln\left(\frac{r}{a} + \sqrt{\frac{r^2}{a^2}+1}\right) - \frac{r}{a}\left(\frac{r^2}{a^2}+1\right)^{-1/2} \right\}, \tag{5.10}$$

a is the scale height in kpc and j_0 is the central luminosity density obtained by I_0/a where I_0 is obtained by fitting the luminosity profile to the Hubble luminosity profile law.

In Eq [5.10], even though the mass is a divergent the potential is a finite quantity and for distances much greater than a it is a point source. Fig [5.1] below shows the rotation curve derived by the procedure described above

Uncertainties and assumptions in the model

The major source of uncertainty arises from the small sample size we have chosen. The reason for doing this has been to keep the sample as homogeneous as possible. The luminosity profile were taken as an average of the major and minor axis profiles. The photometry, especially in the central regions of galaxies is not very clearly resolved. Hence the bulge is rather poorly determined in our model. However, since our aim has been to look at halo properties slightly away from the central region the poor determination of the bulge has not been an important factor.

5.2.2 Dark Matter Potential and Trends in the Halo Parameters

We compute the dark matter potential for each of these galaxies by the prescription outlined in Chapter 2 in a self consistent fashion with the visible matter potential calculated above. Within the context of our model we have two parameters in external galaxies, the central density of the dark matter (ρ_0) and the velocity dispersion $\langle v^2\rangle^{1/2}_{\rm DM}$. When we applied our model to the Galaxy, we had a value for the value of $\rho_{\rm DM} = 0.3\,{\rm GeVcm}^{-3}$. Our aim here is to see if we can constrain the $\rho_{\rm DM} - \langle v^2\rangle^{1/2}_{\rm DM}$ space for the values of V_c. Since V_c is a measure of the mass distribution in the galaxy it will depend on both ρ and the $\langle v^2\rangle^{1/2}_{\rm DM}$.

As a first step we know that the Galaxy with a typical $V_c \approx 250$ kms^{-1}and the Solar neighborhood value of $0.3\,{\rm GeVcm}^{-3}$ and which translates to a value of $1\,{\rm GeVcm}^{-3}$ at the center. We have chosen the values for ρ_0 to vary from $1\,{\rm GeVcm}^{-3}$ to $0.1\,{\rm GeVcm}^{-3}$. The distribution of maximum rotational values range from $V_c = 50$ kms^{-1}to $V_c = 250$ kms^{-1}at typical distances of between 5–15 kpc. In galaxies the centrifugal force is supported by the gravitational force which can be written as

$$\frac{4\pi G\rho R}{3} = \frac{V_c^2}{R} \tag{5.11}$$

Name	$\langle v^2 \rangle_{DM}^{1/2}$	V_c
2259	150	50
2403	450	120
2841	600	300
2903	450	220
3031	450	250
3198	250	150
4236	100	80
4258	300	200
4736	750	200
5033	300	250
5055	750	225
7331	300	225

Table 5.3: We see a correlation between the rotational velocity, V_c and the velocity dispersion $\langle v^2 \rangle_{DM}^{1/2}$

The maximum rotational velocity value can be plugged in for a typical distance to obtain the value of ρ at that point. For our Galaxy, assuming $V_c = 250$ kms^{-1}for a distance of 10 kpc we obtain a value of $\rho \approx 0.113 M_{\odot} pc^{-3}$. This value stands to good comparison with the dynamical estimate of Oort to be $0.114 M_{\odot} pc^{-3}$ at the Solar neighborhood. Since this density seems to be consistent with $0.3\,\mathrm{GeVcm}^{-3}$, we have used the similar criteria to have an order of magnitude estimate. The maximum rotational velocity for each of these galaxies will give an order of magnitude estimate for the density at that distance. Using this criteria the allowed the central densities can vary from $1\,\mathrm{GeVcm}^{-3}$ to $0.1\,\mathrm{GeVcm}^{-3}$.

We have computed the dark matter potential and the rotation curve for all the 12 galaxies. The free parameters are the velocity dispersion ($\langle v^2 \rangle_{DM}^{1/2}$) and the central density (ρ_0) and we notice the following trends In the Fig [5.2] below we show the total rotation curve with the ,dark matter component added to the disk and bulge components for a particular choice of the $\rho_0 = 1\,\mathrm{GeVcm}^{-3}$. For each of the galaxies there is a particular fit of velocity dispersion that we obtain and this is listed in Table [5.3]

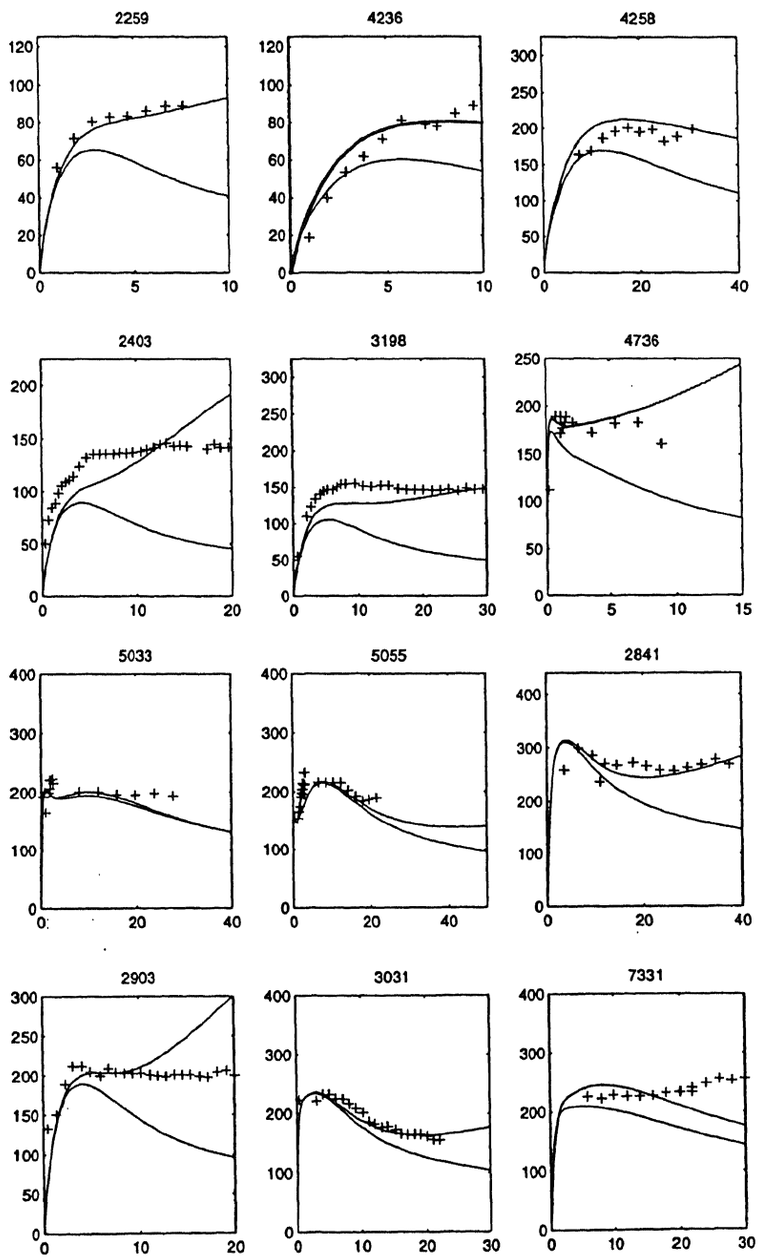

Figure 5.2: The fits to the rotation curves with the the theoretical "visible+dark"rotation curve obtained.

We shown some of the best-fits we have obtained for the 12 galaxies. While most galaxies show a fairly flat or rising curve galaxies like 3031 show a declining rotation curve. There are 2 galaxies with low rotational velocities of 50 kms^{-1}(N4236, U2259) and 4 galaxies(N2403, N3198, N4258, N4736) with rotational speeds of the order of 100 $\mathrm{kms}^{-1}$and the rest of the galaxies have a larger rotational velocity of 200-250 kms^{-1}. Larger the rotational velocity, larger is the velocity dispersion and the density of the dark matter. Fig [5.3] shows the plot of rotational velocity vs velocity dispersion, $\langle v^2\rangle_{\mathrm{DM}}^{1/2}$ for a particular choice of the central density, $\rho_{\mathrm{DM}}(0)$ of $1\,\mathrm{GeVcm}^{-3}$. It should be borne in mind that the sample statistics is too low to make conclusive statements. There are indications that larger rotational speeds correspond to larger dispersions [5.3]. The rotation curve in the central regions of the galaxies are poorly determined and some of them do not have observations out to large distances. It is clear that for larger V_c the velocity dispersion increases for a given central density. We have done the above exercise for a range of densities as previously mentioned. In the usual one-component isothermal description of the dark halo one would expect that for a given rotational speed the dispersion is related by $\langle v^2\rangle_{\mathrm{DM}}^{1/2} = \sqrt{\frac{3}{2}}V_c$, however it clearly deviates from this description as seen from this analysis. This analysis is in confirmation with the earlier work that the visible matter and dark matter together self consistently determine the properties of the dark matter particles.

For most spiral galaxies there is also an observed relation between the luminosity and the amplitude of the rotation curve and we have attempted to reproduce the same. This is the Tully-Fisher relation $L \propto V_c^4$ is also satisfied and this is shown in Fig [5.4]. The Tully-Fisher relation relates the luminosity of the visible matter to the maximum rotational velocity which is a measure of the total potential at a given point. The Tully-Fisher relation is interesting in that it correlates the luminosity which is entirely provided by the visible matter to the $V_{c,max}$ which is a tracer of the total potential. If the dark matter is present at all radii, then there should be a correlation between their distributions. If on the other hand the inner part of the rotation curve is provided by the disk alone then there is some strange disk-halo conspiracy that is at work.

In conclusion we state that the mass modelling of the galaxies confirms the earlier fact that a single component isothermal sphere is perhaps not a good description of galaxies and to determine the properties of the dark matter a self consistent calculation is important.

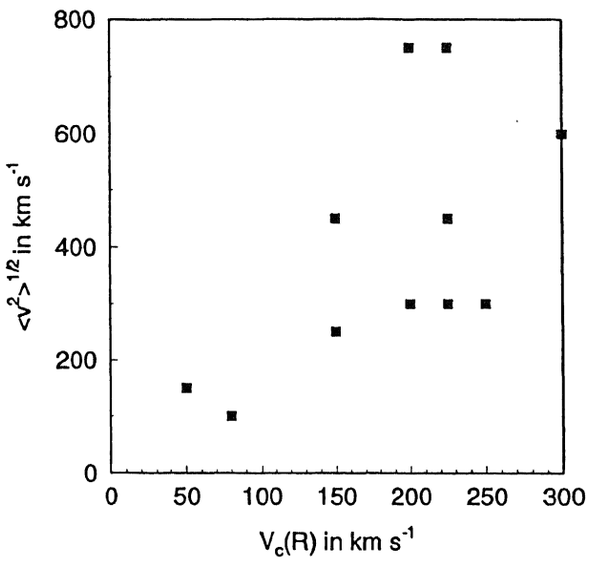

Figure 5.3: This show the correlations between the rotational velocity and velocity dispersion; larger the rotational velocity larger the dark matter velocity dispersion

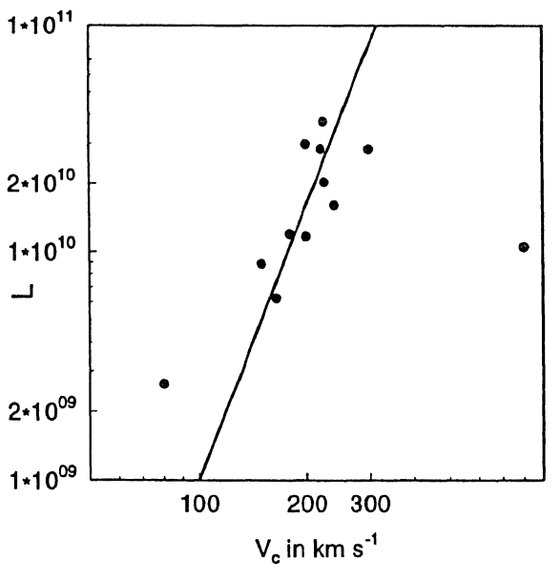

Figure 5.4: The Tully-Fisher relation

Bibliography

[1] Kent, S.M., 1986, A.J., 91, 1301

[2] Thuan, T.X., and Gunn, J.E., 1976, PASP., 88, 543

[3] Athanassoula, E., Bosma, A., & Papaioannou,S., 1987, 179, 23

[4] Bosma, A., Van der Kruit, P.C., 1979, A&A, 79, 281

[5] Albada,T.S.,van, Bahcall, J.N., Begeman, K., and Sancisi, R., 1985, ApJ, 295, 305

[6] DeVacouler's & Pence, 1978, AJ, 83, 1163

[7] Toomre, A., ApJ, 1962, 138, 385

[8] Mihalas, D., & Binney, J.J., 1981, *Galactic Astronomy*, 2^{nd} ed., San Francisco: Freeman

Chapter 6

Conclusions

The Galaxy has two visible components: the bulge and the disk and an unidentified dark halo component whose presence is established solely by its gravitational interaction. This thesis attempts to study properties of the dark matter component using observations which trace the total potential *viz* the rotation curve. We have estimated self-consistently, the contribution of the halo to the rotation curve. Modelling the visible matter in terms of a suitable density distribution and by obtaining the self consistent distribution of the halo, we have determined the velocity dispersion $\langle v^2 \rangle_{\rm DM}^{1/2}$ of the dark matter particles. The value of 600 kms^{-1}that is obtained is twice as large as what is obtained by modelling the Galaxy as a single component isothermal sphere. It is clear that the potential of the visible matter affects the dynamics of the dark matter particles in a non-linear fashion. We have also shown that the specific choice of the distribution function for describing the dark matter component is not crucial to this result.

Dwarf spheroidal galaxies are used to constrain the rotation curve of the Galaxy at large distances. Kinematical constraints based on the spatial distribution of these DSs were imposed on their orbits. We find that there is an anisotropy in their velocity distribution and this anisotropy factor is large and depends on the spatial distribution of the galaxies. Our analysis indicates that there could be a large anisotropy in their velocity distribution so that their observed radial velocities may be interpreted as yielding rotational speeds 300-350 kms^{-1}at galactocentric distances of 100-200 kpc. Note that this is much larger than $V_c \approx 200$ kms^{-1}at the Solar location.

Detection of dark matter involves knowledge about the $\langle v^2 \rangle_{\rm DM}^{1/2}$ and we have studied the consequences of a larger velocity dispersion derived in this thesis. We find that the exclusion region in the mass cross section is increased and the annual and diurnal modulation signals

are much weaker for the larger velocity dispersion. Using the same kind of analysis carried out for the Milky Way we have modelled the mass distribution of 12 galaxies in a similar fashion and find a positive correlation between the rotational velocity and the velocity dispersion. It is clear that even in these galaxies the single component isothermal description will not suffice and the visible matter has an important role to play.

This study has been mainly on non-rotating halos and we have discussed work done by other people on single component rotating halos. However a full calculation would involve including the visible component also. In conclusion we would to state that improved observations of the rotation curve beyond the Solar circle and of the velocities of dwarf spheroidal galaxies and globular clusters would help use probe the phase space structure of the dark matter halo more closely.